Title: A commensal-derived sugar protects against metabolic disease

Authors: Chin Yee Tan[1,2,8], Danting Jiang[1,3], Barbara S. Theriot[1], Meghana V. Rao[1,4], Neeraj K. Surana[1,2,5,6,7]*

Affiliations:

[1]Department of Pediatrics, Duke University School of Medicine; Durham, NC 27710, USA.

[2]Department of Molecular Genetics and Microbiology, Duke University School of Medicine; Durham, NC 27710, USA

[3]Program in Computational Biology and Bioinformatics, Duke University School of Medicine; Durham, NC 27710, USA

[4]Department of Medicine, Duke University School of Medicine; Durham, NC 27710, USA

[5]Department of Integrative Immunobiology, Duke University School of Medicine; Durham, NC 27710, USA

[6]Department of Cell Biology, Duke University School of Medicine; Durham, NC 27710, USA

[7]Duke Microbiome Center, Duke University School of Medicine; Durham, NC 27710, USA

[8]Present address: Duke-NUS Medical School, Singapore 169857

*Lead contact

Correspondence: neil.surana@duke.edu

SUMMARY

Obesity is a worsening global epidemic that is regulated by the microbiota through unknown bacterial factors. We discovered a human-derived commensal bacterium, *Clostridium immunis*, that protects against metabolic disease by secreting a phosphocholine-modified exopolysaccharide. Genetic interruption of the phosphocholine biosynthesis locus (*licABC*) results in a functionally inactive exopolysaccharide, which demonstrates the critical requirement for this phosphocholine moiety. This *C. immunis* exopolysaccharide acts via group 3 innate lymphoid cells and modulating IL-22 levels, which results in a reduction in serum triglycerides, body weight, and visceral adiposity. Importantly, phosphocholine biosynthesis genes are less abundant in humans with obesity or hypertriglyceridemia, findings that suggest the role of bacterial phosphocholine is conserved across mice and humans. These results define a bacterial molecule—and its key structural motif—that regulates host metabolism. More broadly, they highlight how small molecules, such as phosphocholine, may help fine-tune microbiome–immune–metabolism interactions.

KEYWORDS

Microbiome, obesity, metabolic disease, exopolysaccharide, group 3 innate lymphoid cell, phosphocholine, microbe–host interactions

INTRODUCTION

The global obesity epidemic continues to worsen, with over half the world's population estimated to be overweight or obese by 2035[1]. This increase in the prevalence of obesity is estimated to drive sharp increases in cardiometabolic diseases[2,3], such as coronary heart disease, type 2 diabetes, and stroke. Although body mass index (BMI) is frequently used as a diagnostic tool for obesity, it is well documented to be an imperfect measure[4-7]. Instead, excess visceral adipose tissue (VAT)—the hormonally active component of body fat that surrounds the internal organs[8]—is a better predictor for development of metabolic disease[8-11].

While the development of visceral adiposity is complex, it is increasingly recognized that the microbiota plays a critical role in its regulation[12-14]. This idea is rooted in the finding that germ-free animals have less total body fat and visceral fat compared to conventionally raised animals[12], differences that relate to the microbiota harvesting greater amounts of energy from the host diet and promoting the storage of that energy as fat[12,15]. Although early studies demonstrated that the adaptive immune system is not involved in this process[12], more recent work has clarified the requirement of the innate immune system, particularly that of group 3 innate lymphoid cells, in mediating microbiome-dependent enhancement of adiposity[16-19]. However, the specific microbial mechanisms involved in modulating VAT and metabolic diseases are unknown.

Here, we demonstrate that *Clostridium immunis*, a human-derived commensal bacterium we previously found protects against colitis[20], also protects against metabolic disease, with decreases in serum triglyceride levels and VAT. Importantly, we purified and characterized an exopolysaccharide (EPS) as the bioactive molecule required for these metabolic effects, defined the EPS structural motif critical for activity, and elucidated the immunological mechanism of action. Moreover, we used metagenomic analyses to confirm our key findings are generalizable to metabolic disease in humans. Considered together, our study provides new mechanistic insight into how the microbiome regulates VAT and metabolic disease.

RESULTS

C. immunis protects against metabolic disease

In previously published work, we identified *Clostridium immunis*, a newly-discovered human commensal bacterium that protects mice against colitis[20]. To better understand how *C. immunis* protects against colitis, we compared the colonic transcriptional profile of gnotobiotic mice harboring a mouse microbiota (MMb) treated with or without *C. immunis*. Although we did not detect notable changes in immune-related genes, we observed that *C. immunis* treatment surprisingly led to suppression of numerous genes related to lipid uptake and metabolism (Figure S1A). We confirmed these findings extended to the small intestine, the primary site of lipid metabolism, by demonstrating *C. immunis* inhibits small-intestinal expression of *Cd36*, which encodes a transporter that imports fatty acids into cells[21], and *Scd1*, which encodes a stearoyl-coenzyme A desaturase[22] (Figures S1B and S1C). Moreover, we found that *C. immunis* treatment inhibits small-intestinal expression of *Nfil3* (Figure 1A), a microbiota-dependent transcription factor that positively regulates the expression of many of the differentially expressed metabolism-related genes we identified (Figure S1D)[19].

Given that deletion of any of these three genes results in decreased lipid metabolism and reduced VAT[19,22,23], we reasoned that treatment with *C. immunis* may similarly improve metabolic features. Indeed, one week after a single oral treatment with *C. immunis*, mice had significantly lower serum triglyceride levels, reduced body weight, and less gonadal fat (a measure of VAT) than untreated mice (Figures 1B–D). We additionally confirmed *C. immunis* reduces abdominal adiposity via dual energy X-ray absorptiometry (DEXA; Figure 1E). Importantly, these effects of *C. immunis* were not due to differences in food intake or energy expenditure (Figures S2A–F). Moreover, the decrease in VAT does not result from increased lipolysis as serum levels of non-esterified fatty acids and glycerol—two metabolites expected to increase in the setting of lipolysis—are unchanged with *C. immunis* treatment (Figures S1E, S1F).

While these results demonstrate that *C. immunis* improves metabolic disease under short-term, healthy conditions, we investigated whether it also protects against these features in a model of diet-induced obesity (DIO). We orally treated mice with or without *C. immunis* every week for 12 weeks, during which time mice were fed a high-fat diet. While control mice gained ~50% of their body weight during this time, *C. immunis*-treated mice gained significantly less weight (Figures 1F, 1G). In addition, *C. immunis*-treated mice had significantly less gonadal fat at the conclusion of the high-fat diet challenge (Figure 1H). These data demonstrate that *C. immunis* is also effective in the context of long-term DIO. Although the microbiota generally promotes adiposity[19,24], it is notable that treatment with *C. immunis* decreased VAT, even in the presence of a complex microbiota.

A high-molecular weight exopolysaccharide purified from *C. immunis* recapitulates its activity

Intriguingly, neither *Clostridium symbiosum* nor *Clostridium clostridioforme*, two bacterial species that share significant genetic and proteomic similarity with *C. immunis*, respectively (*6*), had any impact on *Nfil3* expression or VAT (Figures 1A and 1D), findings that indicate *C. immunis* has unique functionality compared to these closely related bacterial species. We hypothesized *C. immunis* colonized mice effectively given a single oral dose of *C. immunis* had phenotypic effects that persisted for at least one week. However, while *C. immunis* was detectable in feces 12 hours after administration, it was completely absent by 48 hours (Figure 2A), a finding that suggests the bioactive principle may be present as a pre-formed component within the *C. immunis* culture used for oral treatment. Indeed, mice treated with *C. immunis* conditioned supernatant had decreased small-intestinal expression of *Nfil3* and significantly decreased VAT (Figures 2B and 2C), which confirmed that these metabolic effects are mediated by a molecule secreted by *C. immunis*. Taken together, these data indicate that the activity of *C. immunis* is dependent on a secreted molecule that is lacking in *C. symbiosum* and *C. clostridioforme*.

Accordingly, we performed comparative genomics to identify secreted compounds uniquely produced by *C. immunis*. We initially identified 122 genes that were present in *C. immunis* but absent in both *C. symbiosum* and *C. clostridioforme* (Figure 2D). We manually curated this list to identify those likely to produce extracellular products, which further reduced this list to 30 genes (Figure 2D, Table S1). Intriguingly, nearly one-quarter of these genes were related to biosynthesis of an extracellular polysaccharide, a well-described mechanism by which commensal bacteria modulate host physiology[25-27]. As such, we purified from *C. immunis* supernatant a high-molecular weight exopolysaccharide (EPS; Figure 2E), which contained no appreciable protein, nucleic acid, or lipid contamination (Figures S3A–C). Critically, mice treated with this *C. immunis* EPS—but not EPS purified from *C. symbiosum*—had decreased small-intestinal expression of *Nfil3* and reduced levels of VAT compared to control animals (Figures 2F and 2G). These data conclusively establish that the *C. immunis* EPS is the relevant bioactive molecule that protects against metabolic disease in vivo.

Phosphocholine modification of the *C. immunis* EPS is essential for activity

To understand the structural determinants of activity of *C. immunis* EPS, we performed glycosyl compositional analysis on EPS purified from *C. immunis* and *C. symbiosum*. The overall monosaccharide composition did not differ markedly between the two species, with both EPS structures composed primarily of mannose and glucose (Figure S4A). Although this mannan-like composition is common in plants and fungi, it is rare in bacterial polysaccharides[28,29]. Furthermore, the ^{1}H-NMR spectra for both EPS samples from *C. immunis* and *C. symbiosum* were very similar with respect to the anomeric signals that form the carbohydrate portion (Figure 3A). However, the *C. immunis* EPS contained a narrow signal at 3.22 ppm suggestive of phosphocholine; this sharp singlet is absent in the *C. symbiosum* EPS, which instead has a triplet slightly downfield (Figure 3A). Of note, phosphocholine moieties on polysaccharides (e.g., capsule, lipooligosaccharides) from mucosal pathogens enhance virulence by modulating the host immune system[30], an important precedent for an analogous role that phosphocholine may play in regulating host–commensal interactions. Upon closer examination of the genes identified as distinguishing *C. immunis* from *C. symbiosum* and *C. clostridioforme*, we found two genes that shared homology to a choline transporter (*licB*) and a phosphocholine transferase (*licC*; Table S1). These genes reside in a three-gene operon that also contains a choline kinase (*licA*; Figure S4B).

To determine whether this *licABC* operon is required for activity, we first needed to develop a system to genetically manipulate *C. immunis*, a feat that is still challenging for most commensal organisms[31]. Although CRISPR-Cas9 has been a useful approach to make isogenic mutants in some clostridial species[32,33], expression of Cas9 was toxic to *C. immunis*, similar to its effect in many other commensal bacteria[34]. Instead, we created a suicide plasmid that contained an erythromycin resistance cassette flanked by DNA homologous to *C. immunis licA* to facilitate homologous recombination that disrupted the entire *licABC* locus (Figure S4C).

We isolated EPS from the *C. immunis*Δ*licABC* isogenic mutant ($Ci_{\Delta licABC}$EPS) and found that its monosaccharide composition was similar to that of wild-type *C. immunis* EPS (CiEPS; Figure S4A). Heteronuclear single quantum coherence (HSQC) spectra, which shows the correlation between a carbon and hydrogen bonded directly to it, for both CiEPS and $Ci_{\Delta licABC}$EPS confirmed that the anomeric regions were not significantly different between the two samples (Figure S4D). Combining these data with linkage analysis (Figure S4E), we were able to assign all the anomeric protons in the ^{1}H-NMR (Figure S4F). However, as anticipated, ^{1}H-NMR, HSQC, and correlation spectroscopy (COSY), which reveals correlations between protons that are 2–3 bonds apart, confirmed the absence of phosphocholine in $Ci_{\Delta licABC}$EPS (Figures 3A, 3B, S4G). We further confirmed the absence of phosphocholine in $Ci_{\Delta licABC}$EPS via an immunoblot (Figures 3C, 3D).

Thus, we used 3 orthogonal methods—structural analysis, bacterial genetics, and immunoblotting—to conclusively demonstrate that *C. immunis* EPS contains phosphocholine. Consistent with

phosphocholine being critical for the activity of *C. immunis* EPS, we found that mice treated with $Ci_{\Delta licABC}$EPS had small-intestinal expression of *Nfil3* and levels of adiposity that were indistinguishable from control animals (Figures 3E, 3F). These findings raise the possibility that phosphocholine—even in the absence of the polysaccharide—is sufficient to regulate VAT. However, mice treated with free phosphocholine had similar amounts of VAT as control animals (Figure S4G). Given that neither the phosphocholine-free polysaccharide (i.e., *C. symbiosum* EPS and $Ci_{\Delta licABC}$EPS) nor free phosphocholine can reduce VAT, our data clearly demonstrate that the phosphocholine must be attached to the *C. immunis* EPS for its ability to modulate host metabolism.

C. immunis modulates metabolic disease via ILC3s

Having determined the bacterial mechanism by which *C. immunis* regulates VAT, we sought to define the host mechanisms required for its activity. Recent work established that the microbiota positively regulates *Nfil3* expression and VAT by increasing dendritic cell (DC) secretion of IL-23, which elicits more IL-22 from ILC3s[19]. In our case, *C. immunis* negatively regulates small-intestinal expression of *Nfil3* and the amount of VAT, and we hypothesized these effects are mediated through the same host-mediated pathways. However, we found that IL-23 levels were not altered in *C. immunis*-treated mice (Figures S5A, S5B), which suggests that *C. immunis* may not directly impact DCs. In contrast, we found that *C. immunis* can directly impact ILC3 function. MNK-3 cells, an ILC3-like cell line[35], treated with *C. immunis* had altered expression of *Il22* and *Csf2*, which encodes GM-CSF, with no impact on expression of *Il17a* (Figures S5C–E). Furthermore, CiEPS is sufficient to modulate cytokine expression in MNK-3 cells, and this activity is dependent on phosphocholine (Figures S5F–I). Collectively, these findings support the notion that *C. immunis* EPS can directly modulate ILC3 effector function in a phosphocholine-dependent manner.

To determine whether ILC3s are required in vivo for *C. immunis*-mediated regulation of metabolism, we generated ILC3-deficient mice by breeding $Ahr^{fl/fl}$ mice with *Rorc-cre* mice, as previously described[36]. These ILC3-deficient mice had lower serum triglyceride levels, lower body weights, and reduced amounts of VAT as compared to $Ahr^{fl/fl}$ littermate controls (Figures 4A–C), findings that are consistent with the known role for ILC3s in obesity[19,24,37]. While *C. immunis* treatment of $Ahr^{fl/fl}$ mice phenocopied the effect of ILC3 deficiency, it had no effect in ILC3-deficient mice (Figures 4A–C). Of note, $Ahr^{fl/fl}$ *Rorc-cre* mice also lack *Ahr* expression in T cells[36,38]. Although this has not been found to have significant effects in vivo[39,40], we confirmed our results are not related to T cells by showing *C. immunis* decreases VAT in $Rag1^{-/-}$ mice (Figure 4D). Taken together, these data establish that *C. immunis* decreases VAT in an ILC3-dependent manner.

C. immunis modulates adiposity by decreasing IL-22 levels

Based on our in vitro results with MNK-3 cells, we speculated that *C. immunis* treatment would alter the levels of GM-CSF and IL-22 in vivo given that ILC3s are major sources of these cytokines[41-43]. Interestingly, *C. immunis* treatment led to no significant change in GM-CSF but significantly decreased levels of small-intestinal IL-22 transcript and protein levels (Figures 5A–D). This decreased IL-22 level in vivo is likely more physiologically relevant than the increased *Il22* expression we observed in vitro and may reflect differences in the immune environment between these experimental conditions. Consistent with the lack of change in GM-CSF levels, *C. immunis* retained activity in reducing the amount of VAT in $Csf2rb^{-/-}$ mice that lack the GM-CSF receptor, which demonstrates that GM-CSF signaling is dispensable for *C. immunis*-mediated modulation of adiposity (Figure 5E). In contrast, *C. immunis* lacked activity in mice depleted of IL-22 by a neutralizing antibody (Figure 5F), the activity of which we confirmed by demonstrating reduced expression of *Reg3g* (Figure 5G), a canonical IL-22-dependent gene[42,44]. Considered together, these data establish that *C. immunis* requires ILC3s and IL-22 to protect against metabolic disease.

The abundance of phosphocholine biosynthesis genes is lower in humans with metabolic disease

Given that modification of secreted molecules with phosphocholine is a common strategy by which bacteria in the respiratory tract evade detection and clearance by the host immune system, we postulated that this strategy may also be used by other intestinal commensal bacteria. Using the *C. immunis licABC* gene sequence as a reference, we identified numerous taxonomically diverse gut commensal bacteria that contain a *licABC* locus (Figure 6A). Intriguingly, the gene sequences for bacteria primarily found in the respiratory tract cluster separately from intestinal organisms, which itself forms two distinct clades. Given the phylogeny of the *licABC* gene sequences from the gut commensal bacteria is distinct from the bacterial taxonomic relationships, it is possible the *licABC* locus is spread via horizontal gene transfer. Along these lines, it is interesting to note that the *C. immunis licABC* operon is flanked by mobile genetic elements (Figure S4B), which may help explain why closely related taxa lacked these genes.

To determine whether our findings are generalizable to metabolic disease in humans, we analyzed publicly available shotgun metagenomic data for the abundance of these phosphocholine biosynthesis genes. We focused on *licC*, which generates the critical CTP-phosphocholine substrate required for decoration of bacterial polysaccharides, as this gene is least commonly found in gut commensal bacteria[45]. Analyzing data from 4,145 otherwise healthy individuals for whom BMI data was available[46], we found an overall negative correlation between the abundance of *licC* and BMI (Figure S6A). More specifically, individuals with a normal BMI (< 25 kg/m^2) had a higher abundance of *licC* genes than obese individuals (BMI $\geq$ 30 kg/m^2; Figure 6B). Additionally, using a different collection of 247 individuals for whom serum triglyceride data was available[46], we similarly found an overall negative correlation between the abundance of *licC* and serum triglyceride levels (Figure S6B), with those with normal triglyceride levels (<150 mg/dL) having a higher abundance of *licC* genes than individuals with hypertriglyceridemia ($\geq$200 mg/dL; Figure 6C). Taken together, these results strongly suggest that our murine findings of a *licABC*-modified bacterial compound regulating triglycerides, weight, and VAT are generalizable to humans.

DISCUSSION

Obesity is a deepening global health crisis, with ~4 million deaths worldwide attributed to individuals being overweight or obese[2]. Given increasing recognition that the microbiota is a critical regulator of lipid metabolism and body composition, microbiota-derived therapeutics may provide scalable and cost-effective solutions to metabolic disease. Here we identify and characterize a specific human commensal bacterium-derived EPS that protects against metabolic disease in a phosphocholine-dependent manner.

Although the microbiota generally promotes the expansion of VAT[12], treatment with *C. immunis*—similar to a few other commensal bacteria[47-50]—results in a decreased amount of VAT. This finding highlights the complexity of microbiome-mediated modulation of metabolic conditions where different organisms have completely opposite effects, with the resulting physiologic changes representing an emergent phenotype. Although the specific bacterial mechanism(s) that leads to altered adiposity has not previously been characterized, there are limited examples suggesting bacterial viability and colonization are required for decreasing adiposity[48,49]. In contrast, *C. immunis*, which does not colonize SPF animals when administered as a probiotic, does so by secreting an immunomodulatory EPS into its environment.

Given that bacteria commonly synthesize high-molecular weight polysaccharides that are either released or secreted into its milieu[51], it is not clear what drives specificity in the host response to them. Assuming only 1% of commensal bacteria produce host-accessible polysaccharides, an estimated average molecular weight of 100 kDa for the polysaccharides, and—based on our findings with *C. immunis*—that there is ~0.1 g polysaccharide for every 10^{10} cfu bacteria, there are ~10^9 bacterial polysaccharides per intestinal epithelial cell given current estimates for the number of commensal bacteria and host cells[52]. Even if each of these assumptions were 10–100 fold too high, there would still be an overwhelming number of bacterial polysaccharides per epithelial cell, which begs the question of how the host distinguishes between all these molecules and what—from the bacterial side—drives specificity.

Indeed, polysaccharides are the most chemically diverse molecule: there are >20 “common” constituent sugars (and many more uncommon sugars), variable linkage patterns (α or β) that can occur at different positions on each sugar substituent, and modifications that include other common biological molecules (e.g., lipids, proteins)[53]. Most of this structural diversity remains unexplored. Bacteria are thought to contain the most diverse (and mostly unexplored) polysaccharides[54,55], owing, in part, to the sheer number of different bacterial species, the inclusion of more uncommon sugars, and a diverse array of modifications. Given that these bacterial glycans are often present on the outermost surface, they play critical roles in mediating host–bacterium interactions, where they facilitate colonization, invasion, and modulate the adaptive and innate arms of the immune system[27,55].

We found that *C. immunis* and *C. symbiosum* produced structurally similar, though functionally divergent, EPS molecules that differed primarily in the presence of a phosphocholine moiety. Polysaccharides modified with phosphocholine are present in taxonomically diverse microbes that colonize humans, particularly bacteria that are present in the respiratory tract[30,56,57]. Phosphocholine-containing bacterial polysaccharides contribute to bacterial colonization[58-60], persistence[61,62], and virulence[61,63]. Moreover, they can facilitate both evasion from, and recognition by, the immune system[30,64,65]. Genes in the *lic* operon are responsible for adding phosphocholine to polysaccharides; however, neither the *licABC* locus nor phosphocholine-containing polysaccharides were previously found in clostridial species[30,45]. To better define the role of the phosphocholine moiety in the *C. immunis* EPS, we developed means to genetically manipulate *C. immunis* and inactivated the *licABC* locus. We found that this isogenic mutant, which produces an EPS identical to the parent isolate but lacking phosphocholine, failed to modulate immune responses or visceral adiposity, findings that conclusively demonstrate the critical role for phosphocholine in modulating metabolic disease. Moreover, we were able to leverage these findings to mine publicly

available metagenomic datasets and demonstrate our findings also generalize to metabolic disease in humans.

It is interesting to speculate that the importance of this phosphocholine moiety is related to the fact that it contains both positively (i.e., choline) and negatively charged (i.e., phosphate) groups. Bacterial polysaccharides are generally neutral or negatively charged, with few containing a positive charge[27,66]. However, bacterial polysaccharides that contain a zwitterionic motif like the *C. immunis* EPS are known to modulate the immune system[66-69]. *Bacteroides fragilis* polysaccharide A is the archetypal example of an immunomodulatory zwitterionic polysaccharide (ZPS), where chemical neutralization of either charged group results in a functionally inactive molecule[66]. These previously described ZPSs are presented via the MHCII pathway such that they activate $CD4^+$ T cells[69,70]. In contrast, our in vitro findings suggest that the *C. immunis* EPS may directly modulate the function of ILC3s in a manner dependent on its zwitterionic phosphocholine moiety.

Specifically, *C. immunis*-treated mice have decreased small-intestinal levels of IL-22, one of the canonical ILC3 cytokines. Moreover, antibody-mediated neutralization of IL-22 abrogates the effect of *C. immunis*, a finding that demonstrates that modulation of IL-22 levels is central to *C. immunis*-mediated protection against metabolic disease. Although IL-22 is generally regarded as a key cytokine in regulating VAT, there is ongoing controversy regarding its specific role. While some studies have found IL-22 protects against metabolic disease[18,71], others have found that it promotes metabolic dysfunction[19,24,72]. In contrast, *Il22*$^{-/-}$ mice had no metabolic phenotypes[73,74], a finding that suggests IL-22 may not be essential to metabolic health. These discrepancies may relate to differences in IL-22 levels in the different model systems, with persistent, high-levels of IL-22 leading to protective phenotypes[18,74], whereas transient, low-levels of IL-22 had disease-promoting roles[19]. The effects we observe with *C. immunis* EPS may fall into this latter category, with the transient decrease in endogenous IL-22 leading to disease protection.

Our identification of *licABC* as the bacterial genes required for activity of the *C. immunis* EPS enabled us to identify this operon in many other commensal gut bacteria. These gut bacterial *licABC* genes may have eluded prior identification given their sequences are quite distinct from that of respiratory pathogens, in which *licABC* genes have been extensively characterized[30]. It is likely that these other gut commensal bacteria decorate some surface-associated molecule with phosphocholine, similar to what has been observed with *licABC*-containing respiratory pathogens[30]. It is possible that modification of common commensal-associated molecular patterns with small haptens, such as phosphocholine, may help create a “combinatorial code” that provides increased specificity to host–microbiota interactions and thus fine-tunes physiological perturbations.

Considered together, our work couples biochemical and genetic approaches to characterize a commensal bacterium-derived, phosphocholine-containing EPS that protects against metabolic disease in an ILC3-dependent manner. Our findings offer the possibility for microbiota-derived products that treat obesity and related comorbidities. More broadly, our work highlights that as the ability to culture and genetically manipulate commensal organisms continues to advance, demonstrating the genetic and structural basis for how the microbiota impacts host physiology will become more commonplace, just as it has become de rigueur in microbial pathogenesis.

ACKNOWLEDGEMENTS

We thank the Duke Gnotobiotic Core, the DLAR Breeding Core, and the Sequencing and Genomic Technologies Core for technical assistance; Dustin R. Middleton for advice on polysaccharide enrichment; and the Complex Carbohydrate Research Center (University of Georgia), which is supported by the US Department of Energy under award DE-SC0015662, for performing structural analyses of purified exopolysaccharides. CYT received support from American Heart Association pre-doctoral fellowship AHA 897275, a National University of Singapore Development Grant, a Tan Kah Kee Postgraduate Scholarship, and a Triangle Center for Evolutionary Medicine Graduate Student Award. NKS received support from NIH awards R03 AI142341 and P30 DK034987, the Hartwell Foundation Individual Biomedical Research Award, and as a Duke Translating Duke Health Scholar and a Whitehead Scholar.

AUTHOR CONTRIBUTIONS

Conceptualization: CYT, NKS

Methodology: CYT, DJ, BST, NKS

Investigation: CYT, MVR

Formal analysis: DJ

Visualization: CYT, NKS

Funding acquisition: CYT, NKS

Project administration: CYT, NKS

Supervision: NKS

Writing – original draft: CYT, NKS

Writing – review & editing: CYT, DJ, BST, MVR, NKS

DECLARATION OF INTERESTS

N.K.S. is an inventor on patent applications 16/312,815 and 16/625,217 submitted by Harvard University that cover the therapeutic use of *C. immunis*. C.Y.T and N.K.S. are inventors on a patent application submitted by Duke University that covers the therapeutic use of the *C. immunis* exopolysaccharide.

SUPPLEMENTAL INFORMATION

Document S1. Figures S1–S6 and Table S1

FIGURE LEGENDS

Figure 1: *C. immunis* protects against metabolic disease. (**A**) Quantitative PCR (qPCR) analysis of small-intestinal *Nfil3* expression from MMb mice treated orally with or without the indicated bacteria (n = 4–8 mice per group). (**B–E**) Mice were orally treated with or without the indicated bacteria. One week later, serum triglycerides (**B**; 6–9 mice per group), body weight (**C**; n = 10–13 mice per group), gonadal fat mass normalized to body weight (**D**; n = 4–6 mice per group), and percent abdominal fat measured via a DEXA scan were assessed (**E**; n = 5–6 mice per group). (**F–H**) Longitudinal weights for SPF mice fed a high-fat diet and orally treated with or without *C. immunis* each week (**F**; n = 7–8 mice per group), with the area under the curve shown (**G**). After 12 weeks of the high-fat diet, gonadal fat mass normalized to body mass was assessed (**H**; n = 7–8 mice per group). Data are represented as mean±s.e.m. *P < 0.05; **P < 0.01; ns, not significant by one-way ANOVA with Holm-Šidák correction (**A, D**) or Mann-Whitney (**B, C, E, G, H**). See also Figures S1 and S2.

Figure 2: A high-molecular weight exopolysaccharide purified from *C. immunis* recapitulates its activity. (**A**) Longitudinal qPCR analysis of *C. immunis* fecal abundance in mice orally treated with 10^7 CFU of *C. immunis.* (n = 10 mice). (**B, C**) C57BL/6 mice were treated orally with or without conditioned supernatant from *C. immunis*, with qPCR analysis of small-intestinal *Nfil3* expression (**B**; n = 9 mice per group) and gonadal fat mass normalized to body weight assessed (**C**; n = 8 mice per group). (**D**) Schematic of comparative genomic analysis for *C. immunis* genes associated with activity. (**E**) Periodic acid–Schiff-stained SDS-PAGE gel of a control, *C. immunis* supernatant, and purified *C. immunis* exopolysaccharide (EPS). The control consisted of sterile bacterial media that went through the same purification process as *C. immunis* EPS, and all samples represent an equal amount of culture volume. (**F, G**) C57BL/6 mice were treated orally with or without EPS purified from the indicated bacteria, and qPCR analysis of small-intestinal *Nfil3* expression (**F**; n = 3–7 mice per group) and gonadal fat mass normalized to body weight was assessed (**G**; n = 6 mice per group). Data are represented as mean±s.e.m. *P < 0.05; ****P < 0.0001; ns, not significant by unpaired Student's t test (**B, C**) or one-way ANOVA with Holm-Šidák correction (**F, G**). See also Figure S3

Figure 3: Phosphocholine modification of *C. immunis* EPS is essential for activity. (A) ^{1}H-NMR spectra of EPS purified from *C. immunis, C. symbiosum*, or *C. immunisΔlicABC*. The arrow highlights a peak corresponding to phosphocholine, which is only present in EPS from *C. immunis*. **(B)** Zoomed region of 2D-COSY spectra of the *C. immunis* (left) and *C. immunis*$_{\Delta licABC}$ EPS (right) highlighting the cross peak for two of the phosphocholine protons, which is absent in the *C. immunis*$_{\Delta licABC}$ EPS. **(C)** Immunoblot of CiEPS and Ci$_{\Delta licABC}$EPS that is probed with an antibody against phosphocholine (anti-ChoP; top blot). Samples were also visualized with periodic acid–Schiff stain (PAS; bottom blot). **(D)** Quantification of the band intensities in panel (C), with values from the immunoblot normalized to that from the PAS-stained blot. (**E, F**) C57BL/6 mice were treated orally with a control (sterile culture media), CiEPS, or Ci$_{\Delta licABC}$EPS, with qPCR analysis of small-intestinal *Nfil3* expression (**E**; n = 3–7 mice per group) or gonadal fat mass normalized to body weight (**F**; n = 6–8 mice per group). Data are represented as mean±s.e.m. *P < 0.05; **P < 0.01; ns, not significant by unpaired Student's t test (**D**), one-way ANOVA with Holm-Šidák correction (**E, F**). See also Figure S4.

Figure 4: *C. immunis* modulates metabolic disease via ILC3s. (A–C) *Ahr*$^{fl/fl}$ (ILC3-sufficient) and *Ahr*$^{fl/fl}$ *Rorc-cre* mice (ILC3-deficient) were orally treated with or without *C. immunis*, with serum triglycerides (**A**; n = 9–10 mice per group), body weights (**B**; n = 10–19 mice per group), and gonadal fat mass normalized to body weight (**C**; n = 5–10 mice per group) assessed one week later. **(D)** *Rag1*$^{-/-}$ mice were orally treated with or without *C. immunis*, and gonadal fat mass normalized to body weight was assessed one week later (n =7–8 mice per group). Data are represented as mean±s.e.m. *P < 0.05; **P < 0.01;

***$P < 0.001$; ns, not significant by ANOVA with Holm-Šidák correction (**A–C**) or unpaired Student's t test (**D**). See also Figure S5.

Figure 5: *C. immunis* modulates adiposity by decreasing IL-22 levels. (A–D) C57BL/6 mice were treated orally with or without *C. immunis*. One week later, qPCR analysis of *Csf2* expression (**A**, $n = 5$ mice per group) and *Il22* (**C**, $n = 6–7$ mice per group) was performed using small-intestinal tissue. ELISA analysis of GM-CSF (**B**, $n = 4–5$ mice per group) and IL-22 (**D**, $n = 5$ mice per group) was performed in ileal biopsy samples from these mice. **(E, F)** Gonadal fat mass normalized to body weight in control and *C. immunis*-treated *Csf2rb*$^{-/-}$ mice (**E**; $n = 11$ mice per group) and C57BL/6 mice treated with an IL-22 neutralizing antibody (**F**; $n = 8$ mice per group). **(G)** qPCR analysis of *Reg3g* in ileal tissue obtained from mice treated with an isotype control or an IL-22 neutralizing antibody. Data are represented as mean±s.e.m. *$P < 0.05$; ****$P < 0.0001$; ns, not significant by Mann-Whitney test (**A–D**), or unpaired Student's t test (**E–G**).

Figure 6: The abundance of phosphocholine biosynthesis genes is lower in humans with metabolic disease. (A) A randomized axelerated maximum likelihood (RAxML) phylogenetic tree depicting *licABC* genes identified in *C. immunis* and other gut commensal bacteria is shown, with the *licABC* genes from four bacteria primarily found in the respiratory tract added in for reference. **(B)** The abundance of *licC* in human fecal metagenomic data is shown for individuals with a healthy (< 25 kg/m^2; $n = 2021$) or obese BMI (≥ 30 kg/m^2; $n = 816$). **(C)** The abundance of *licC* in human fecal metagenomic data is shown for individuals with normal (<150 mg/dL; $n = 193$) or high serum levels of triglycerides (≥200 mg/dL; $n = 22$). Data are represented as mean±s.e.m. *$P < 0.05$; ****$P < 0.0001$ by Mann-Whitney test (**B, C**). See also Figure S6.

SUPPLEMENTARY FIGURE LEGENDS

Figure S1. *C. immunis* inhibits intestinal expression of lipid metabolism genes without increasing lipolysis, related to Figure 1. (**A**) Volcano plot depicting differentially expressed genes in colonic tissue of MMb mice treated orally with or without *C. immunis* (*n* = 3 mice per group). Genes highlighted in red are related to lipid uptake and metabolism. (**B–C**) qPCR analysis of small-intestinal *Scd1* (**B**) and *Cd36* expression (**C**) from MMb mice treated orally with or without *C. immunis* (*n* = 4–7 mice per group). (**D**) Gene set enrichment analysis for NFIL3-dependent genes in the RNAseq dataset depicted in panel A. NES, normalized enrichment score. (**E, F**) C57BL/6 mice were orally treated with or without *C. immunis*. One week later, serum non-esterified fatty acid (**E**; 6–9 mice per group) and glycerol levels (**F**; 6–9 mice per group) were assessed. Data are represented as mean±s.e.m. **P* < 0.05; ns, not significant by unpaired Student's t test (**B, C, E, F**).

Figure S2. *C. immunis* does not impact food intake or energy expenditure, related to Figure 1. Metabolic cage studies for C57BL/6 mice orally treated with or without *C. immunis*. Food consumption (**A**), ambulatory activity (**B**), respiratory exchange ratio (**C**), energy expenditure (**D**), O_2 consumption (**E**), and CO_2 production (**F**) are shown, with data presented for the entire day and by light/dark cycle. None of the data were statistically significant by ANCOVA testing. (*n* = 8 mice per group).

Figure S3. Purified *C. immunis* EPS is devoid of significant protein, nucleic acid, or lipid contamination, related to Figure 2. (**A**) Silver-stained SDS-PAGE of a control, *C. immunis* supernatant, and *C. immunis* EPS. The control included sterile bacterial media that went through the same purification process as *C. immunis* EPS, and all samples represent an equal amount of culture volume. (**B**) Safe DNA-stained agarose gel of *C. immunis* EPS. Two different amounts of the ladder were included to demonstrate sensitivity. (**C**) Sudan Black B-stained PAGE gel of *E. coli* lipopolysaccharide and *C. immunis* EPS.

Figure S4. The polysaccharide components of the CiEPS and $Ci_{\Delta licABC}$EPS are largely similar, related to Figure 3. (**A**) Glycosyl composition analysis of EPS isolated from *C. immunis*, *C. symbiosum*, and *C. immunis* Δ*licABC*. (**B**) A schematic of the *C. immunis* genetic locus containing *licABC* and flanking genes. The predicted promoter is indicated by the arrow. (**C**) A schematic of the genetic strategy used to delete *licABC* in *C. immunis*. *E. coli* was used to conjugally transfer into *C. immunis* a suicide plasmid containing an erythromycin resistance gene (*ErmB*) flanked by homology arrows to *licA*. Erythromycin-resistant (Ery^R) *C. immunis* mutants contained the *ErmB* gene and an 80-bp deletion in *licA*. (**D**) Anomeric regions in the HSQC spectra of CiEPS (left) and $Ci_{\Delta licABC}$EPS (right). The anomeric CH are labelled with letters in the *C. immunis* EPS spectra. (**E**) Linkage analysis of EPS isolated from *C. immunis* and *C. immunis* Δ*licABC*. (**F**) Zoomed anomeric region in the ^{1}H NMR spectra of *C. immunis* (top) and *C. immunis*$_{\Delta licABC}$ EPS (bottom), with tentative assignments of the anomeric protons (as labeled in panel D). Superscript a and b denote residues within a linear or branched region, respectively. (**G**) HSQC spectra of CiEPS (left) and $Ci_{\Delta licABC}$EPS (right) that highlight the C-H interactions from the phosphocholine moiety. The dashed circles in the $Ci_{\Delta licABC}$EPS spectrum reveals where these interactions should appear if the phosphocholine were present. (**H**) C57BL/6 mice were orally administered water (control) or phosphocholine (ChoP), with the gonadal fat mass normalized to body weight assessed one week later (*n*=7–8 mice/group). ns, not significant by Student's t test.

Figure S5. The CiEPS can directly modulate ILC3 effector function in vitro, related to Figure 4. (**A, B**) qPCR (**A**) and ELISA (**B**) analysis of IL-23 in intestinal tissue of mice orally treated with or without *C. immunis* (*n* = 5–6 mice per group). (**C–I**) qPCR analysis of the indicated cytokine genes in MNK-3 cells treated with or without *C. immunis* (**C–E, H, I**), CiEPS (**F, G**), or *C. immunis*Δ*licABC* (**H, I**). **P* < 0.05; ***P*

< 0.01; ns, not significant by Mann Whitney U test (**A–G**) or one-way ANOVA with Holm-Šidák correction (**H, I**).

Figure S6. The abundance of the *licC* gene in fecal metagenomic data is negatively correlated with metabolic disease in humans, related to Figure 6. (**A**) The abundance of *licC* gene copies is plotted against the individual's BMI (n = 4,145). (**B**) The abundance of *licC* gene copies is plotted against the individual's serum triglyceride level (n = 247). The Spearman's ρ and p values are shown for each panel.

STAR METHODS

Mice

C57BL/6J (stock #000664), *Ahr*$^{fl/fl}$ (stock #006203)[75], *Rorc-cre* (stock #022791)[38], and *Rag1*$^{-/-}$ mice (stock #002216)[76] were initially obtained from The Jackson Laboratory. *Csf2rb*$^{-/-}$ mice were obtained from Mari Shinohara (Duke University)[77]. Gnotobiotic Swiss Webster MMb mice were obtained from Dennis Kasper (Harvard University)[78]; these mice were co-housed with germ-free C57BL/6 mice to generate C57BL/6 MMb mice. All animals were bred and maintained in the animal facility at Duke University, and the gnotobiotic mice were bred and maintained in vinyl isolators in the Duke Gnotobiotic Core. Experimental manipulation of gnotobiotic mice was performed in autoclaved, individually ventilated cages in which animals received autoclaved food (LabDiet 5K67) and water. In some experiments, mice were fed a high-fat diet (TestDiet Western Diet AIN-76A; 4.49 kcal/g; 40% of calories from fat). Mice used in experiments were sex- and age-matched and drawn randomly from the same litter, when feasible. All procedures were approved by Duke's Institutional Animal Care and Use Committee and were conducted in accordance with National Institutes of Health guidelines.

Bacteria

C. immunis was obtained from Dennis Kasper (Harvard University)[20]. *C. immunis*, *C. symbiosum* (DSM 29356), and *C. clostridioforme* (DSM 933) were grown in peptone yeast glucose (PYG) broth (Anaerobe Systems) or on brain heart infusion-supplemented (BHI-S) agar plates (ATCC Medium 1293). All clostridial strains were grown in an anaerobic chamber (Coy laboratories) with 2.5% H_2 and 0 ppm O_2 at 37 °C. *Escherichia coli* S17λPir was grown aerobically in LB at 37°C.

RNA-sequencing and analysis

One week after orally administering *C. immunis* (200 μl containing ~10^8 colony-forming units [CFU]) or, as a control, sterile PYG media (200 μl) to male C57BL/6 MMb mice (12 weeks of age), the proximal 2 cm of colon was collected, frozen immediately in liquid nitrogen, and stored at –80 °C until needed. Tissues were homogenized in Trizol (Invitrogen) using a bead-beating approach, and RNA was purified according to the manufacturer's instructions. RNA Integrity Number (RIN) scores for all samples used for RNA-seq were >7.0 as assessed on a TapeStation 2200 (Agilent). cDNA libraries were generated using a mRNA HyperPrep kit (KAPA) and sequenced on a NovaSeq6000 (Illumina; S4 flow cell with 150bp paired-end reads).

FastQC (version 0.11.9) was used to assess read quality and to perform trimming, STAR (release 2.7.9a) was used to align reads to the mouse genome mm10 (GRCm39)[79], and FeatureCounts was used to generate a count table[80]. Differential gene analysis was performed with DESeq2 (version 1.28.1)[81], and a volcano plot was generated with EnhancedVolcano. A preranked gene set enrichment analysis was performed using GSEA 4.3.2 using a previously described NFIL3-dependent gene set as input[19,82]. R (version 4.0.0) was used for all analyses.

Real-time qPCR analysis

RNA was isolated from tissue as described above. For cells, Trizol was added to samples, and RNA was purified according to the manufacturer's instructions. cDNA was prepared using random hexamers and the High-Capacity cDNA synthesis kit (Applied Biosystems), and qPCR was performed on a Step One Real Time PCR system (Applied Biosystems) with iTaq Universal SYBR Green Supermix (Bio-Rad). The following primers were used: *Gadph* fwd: ACCACAGTCCATGCCATCAC; *Gadph* rev: TCCACCACCCTGTTGCTGTA; *Nfil3* fwd: CTTTCAGGACTACCAGACATCCAA; *Nfil3* rev: GATGCAACTTCCGGCTACCA; *Cd36* fwd: TCATATTGTGCTTGCAAATCCAA; *Cd36* rev: TGTAGATCGGCTTTACCAAAGATG; *Scd1* fwd: CTTCTTCTCTCACGTGGGTTG; *Scd1* rev: CGGGCTTGTAGTACCTCCTC; *Il23* fwd: CATGCTAGCCTGGAACGCACAT; *Il23* rev: ACTGGCTGTTGTCCTTGAGTCC; *Il22* fwd: GCTTGAGGTGTCCAACTTCCAG; *Il22* rev:

ACTCCTCGGAACAGTTTCTCCC; *Csf2* fwd: AACCTCCTGGATGACATGCCTG; *Csf2* rev: AAATTGCCCCGTAGACCCTGCT; *Il17a* fwd: ATCCCTCAAAGCTCAGCGTGTC; *Il17a* rev: GGGTCTTCATTGCGGTGGAGAG; *Reg3g* fwd: CCTTCCTCTTCCTCAGGCAAT; *Reg3g* rev: TAATTCTCTCTCCACTTCAGAAATCCT. The comparative Ct method was used to quantify transcripts that were normalized with respect to *Gapdh*. For assessment of *C. immunis* persistence in mice, fecal DNA was isolated as previously described[20], and qPCR was performed using the following primers: *C. immunis* fwd: TACAACTACTCTACCACATTGACTT; *C. immunis* rev: GCGGCGGGTTTAATTTCAGA; Universal fwd: CCTACGGGAGGCAGCAG; Universal rev: ATTACCGCGGCTGCTGGCA. The comparative Ct method was used to quantify transcripts that were normalized with respect to the universal primer results.

Assessment of adiposity and serum chemistries

Mice (13–18 weeks of age) were orally administered either ~10^8 CFU of bacteria, 200 μl of conditioned bacterial supernatant, 4 mg of exopolysaccharide, or sterile PYG media. One week later, serum and the gonadal fat pads were collected. The fat pads surrounding the ovaries and fallopian tubes were collected in female mice, while the epididymal fat pads were collected in male mice. The weight of these gonadal fat pads was normalized to the animal's body weight at time of sacrifice. Serum chemistries (i.e., triglycerides, non-esterified fatty acids, glycerol) were assessed in the Hormone and Conventional Analyte Lab in the Duke Molecular Physiology Institute. Dual energy X-ray absorptiometry (DEXA) experiments were performed in the Biomedical Research Imaging Center at the University of North Carolina, Chapel Hill using a Lunar PIXImus (GE Lunar Corp.), with images gated on the abdominal region. In experiments assessing the impact of *C. immunis* in the context of a high-fat diet, mice were orally administered either ~10^8 CFU of bacteria or sterile PYG media each week, and serum and gonadal fat was collected after 12 weeks.

Indirect calorimetry studies

We performed indirect calorimetry studies of mice orally treated with or without *C. immunis* as well as ILC3-deficient littermate mice treated without *C. immunis* (*n*=8 male mice/group; ~20 weeks of age). These studies were performed in Duke's Mouse Behavioral and Neuroendocrine Analysis Core Facility. Mice received standard chow (LabDiet 5053; 3.43 kcal/g; 13% of calories from fat) and were treated with either sterile bacterial media (control) or ~10^7 cfu of *C. immunis* one week prior to and at the onset of being placed into metabolic cages (Oxymax/CLAMS; Columbus Instruments), where they were monitored for 6 days. Data were analyzed in CalR[83], and statistical analysis was performed using analysis of covariance (ANCOVA) testing and generalized linear models as implemented in CalR.

Genomic comparisons of *Clostridium* species

Genomic DNA was isolated from overnight cultures of *C. immunis*, *C. symbiosum*, and *C. clostridioforme* using a MagAttract HMW DNA kit (Qiagen). A multiplexed sequencing library was generated using a SMRTbell prep kit (PacBio) and sequenced on a PacBio RS. Flye (release 2.8.3) was used to perform de novo assembly on quality-filtered reads[84], which resulted in a complete and circularized genome for *C. immunis* (genome size of 5.34 Mbp), 108 contigs (genome size of 5.54 Mbp) for *C. symbiosum*, and 18 contigs (genome size of 5.84 Mbp) for *C. clostridioforme*. Gene annotation was performed with RAST[85], and a genome-wide, sequence-based comparison of the three strains was performed using The SEED Viewer web server (version 2.0)[84]. Genes that were uniquely present in *C. immunis* were further manually curated to identify genes that are likely to generate extracellular products.

EPS purification

The supernatant from overnight bacterial cultures was concentrated ~50-fold using a 100 kDa molecular weight cutoff (MWCO) spin column (Amicon Ultra, Millipore). The retentate was incubated overnight with DNase I (50 μg/ml) and Rnase A (50 μg/ml) at 37 °C followed by an overnight incubation with proteinase K (500 μg/ml) at 37 °C. The volume of the resultant mixture was increased to 15 ml with dH_2O and

concentrated back down to 1–2 ml using a 100 kDa MWCO column to remove proteinase K. The retentate was precipitated with ice-cold ethanol (80% final volume) at –20 °C overnight. Precipitates were air-dried and resuspended in distilled water.

Visualization of EPS by gel electrophoresis

EPS (60 μg) was boiled for 5 mins in Laemmli buffer with β-mercaptoethanol and run on a 10% polyacrylamide gel (MiniPROTEAN TGX, BioRad) at 200 V for 1hr. Gels were visualized with a silver (Thermo Fisher Pierce), Sudan Black B (Thomas Scientific), or periodic acid–Schiff (PAS) stain. For PAS staining, the gel was washed in deionized water for 10 min, fixed in 12.5% trichloroacetic acid for 30 min, oxidized with 1% periodic acid for 1 h, washed in deionized water for 4–5 h, and stained with Schiff's reagent for 1 h. After staining, the gel was reduced with three 10 min washes in 0.5% sodium metabisulfite. For the Sudan black B-stained gel, *E. coli* 055:B5 lipopolysaccharide (75 μg; Sigma) was used as a positive control. To assess the presence of nucleic acids, EPS (60ug) was run on a 1% agarose gel stained with a DNA Gel Stain (ApexBio) and imaged on an Odyssey XF system (LI-COR Biosciences).

Glycosyl composition analysis

Glycosyl composition analysis was performed by combined gas chromatography-mass spectrometry (GC-MS) of the per-*O*-trimethylsilyl (TMS) derivatives of the monosaccharide methyl glycosides produced from the sample by acidic methanolysis as described previously[86]. Briefly, samples (150–300 μg) were heated with 1 M methanolic HCl in a sealed screw-top glass test tube for 18 h at 80 °C. After cooling and removal of the solvent under a stream of nitrogen, the samples were re-N-acetylated and dried again. The samples were then derivatized with Tri-Sil® (Pierce) at 80 °C for 30 min. GC-MS analysis of the TMS methyl glycosides was performed on an Agilent 7890A GC interfaced to a 5975C MSD, using a Supelco Equity-1 fused silica capillary column (30 m × 0.25 mm ID).

Glycosyl linkage analysis

Glycosyl linkage analysis was performed as previously described[87]. Briefly, samples were dissolved in anhydrous DMSO overnight, and permethylation was achieved by two rounds of treatment with sodium hydroxide base (15 min) and iodomethane (25 min). The permethylated materials were hydrolyzed with 2 M TFA for 2 h at 121 °C and dried down with isopropanol under a stream of nitrogen. The samples were then reduced with 10 mg/mL $NaBD_4$ in 100 mM NH_4OH overnight, neutralized with glacial acetic acid, and dried with methanol. Finally, the samples were O-acetylated using 250 μL of acetic anhydride and 250 μL of concentrated trifluoroacetic acid (TFA) at 45 °C. The samples were dried under N_2 stream, reconstituted in dichloromethane, and washed with nanopure water. The resulting partially methylated alditol acetates were analyzed on an Agilent 7890A GC interfaced to a 5975C MSD; separation was performed on a Supelco 2331 fused silica capillary column (30 m × 0.25 mm ID).

^{1}H-NMR spectroscopy

Each lyophilized EPS sample (~1–2 mg) was dissolved in 500 μl of D_2O (99.9% D, Sigma) and placed in a 5-mm NMR tube. Sodium trimethylsilylpropanesulfonate (0.5 μl) was added as a reference. Liquid ^{1}H-NMR data were obtained at 298 K on a Varian VNMRS spectrometer (1H, 599.66 MHz). ^{1}H-NMR parameters: 2.0 s relaxation delay, 65536 Hz spectral width, 16384 data points and 64 transients with total recycle delay of 3.3 s between each transient. The experiment was performed with suppression of the HOD signal at 4.78 ppm by presaturation. Prior to the Fourier transformation, the data were apodized with an exponential decay function with line broadening of 0.5 Hz, 90º sine square, and zero-filled to 64k points. The baselines were corrected automatically by subtracting a 3rd-order Bernstein polynomial fit. The spectra were processed and analyzed with MestreNova (version 14.2.1-27684).

2D NMR spectroscopy

EPS samples were dissolved in 1.0 ml of D_2O (99.9 % D) and lyophilized. The samples were then dissolved in 0.5 ml of D_2O with 2 µL of 50mM d6-DSS and transferred to 5-mm NMR tubes. All NMR data were acquired at 70 °C on a Bruker Avance III spectrometer (1H, 600.06 MHz) equipped with a cryoprobe using standard pulse sequences. A ^{1}H spectrum was acquired using a standard pulse program with a spectral width of 9615.4 Hz, 32768 data points, and sixteen transients with a total recycle delay of 2 s. For the 2D HSQC experiments, 1H spectral widths were set to 72111.5 Hz and 13C spectral width to 10563.98 Hz. The 2D COSY spectrum was acquired with 8 transients per 400 increments. Chemical shifts were referenced to DSS (δH = 0.00 ppm and δC = 0.00 ppm). The spectra were processed and analyzed with MestreNova (version 14.0.1-23559).

Slot immunoblot

EPS (5 µg) was added to a methanol-activated PVDF membrane housed in a slot blot manifold (Hoefer Inc.). The membrane was blocked in 3% bovine serum albumin in TBS containing 0.1% Tween 20 (TBS-T) for 1 h, followed by overnight incubation at 4 °C with an anti-phosphocholine antibody (1:500 dilution; clone BH8; Millipore). After washing with TBS-T, the membrane was incubated with an HRP-conjugated secondary antibody (Thermo Fisher Scientific) for 1 h. Chemiluminescence generated by treatment with Clarity ECL (Bio-Rad) was imaged on an Odyssey XF system (LI-COR Biosciences). EPS-treated membranes were also stained with PAS as detailed above to visualize the amount of carbohydrate loaded.

Generation of *C. immunis*Δ*licABC*

We established that pMTL82151, one of the ClosTron plasmids[88], fails to replicate in *C. immunis* and therefore could be used as a suicide vector. We used the Q5 High-Fidelity DNA polymerase (NEB) to PCR amplify the *ermB* gene that provides resistance to erythromycin (using pMTL83251 as the template) and two 800 bp regions (separated by 80 bp) that flanked the *licA* target site. PCR primers used are as follows: licA Left fwd: gctcggtacccggggatcctAATACCGTCAGCTACACTG; licA Left rev: cttcggccggTAGGCCGGACATATTCTATATC; licA Right fwd: gaatgtgtttTTTCTATATGGTGATCTTAGTAAAC; licA Right rev: agcttgcatgtctgcaggccTTTAATTGGACAAAGCGTC; ermB fwd: gtccggcctaCCGGCCGAAGCAAACTTAAG; ermB rev: catatagaaaAAACACATTCCCTTTAGTAACGTG. After digesting these three PCR products with XbaI and XhoI, they were cloned into an XbaI- and XhoI-digested pMTL82151 plasmid using HiFi assembly (NEB). Electrocompetent *E. coli* S17λPir was transformed with the ligation mixture, which generated S17λPir:pMTL82151ΔlicABC. This strain was used to transfer pMTL82151ΔlicABC into *C. immunis* using standard conjugation methods. Overnight cultures of *E. coli* donors and *C. immunis* recipients were mixed at a 10:1 donor-to-recipient ratio. Multiple aliquots (30 µl) of the mixture were spotted onto a BHI-S agar plate and incubated anaerobically at 37 °C. After 24–48 h, the total growth on each plate was collected, resuspended in fresh media, and grown on BHI-S plates containing erythromycin (500 µg/ml) and colistin (10 µg/ml). To confirm that the plasmid was not present in *C. immunis*, the culture was also grown on BHI-S plates containing colistin (10 µg/ml) and chloramphenicol (12.5 µg/ml), against which the plasmid backbone confers resistance. Erythromycin-resistant colonies of *C. immunis* were confirmed to harbor the insertion of the *ermB* gene and expected 80-bp deletion in *licA* by PCR and Sanger sequencing.

Cell culture

All tissues and cells were cultured in a humidified incubator with 5% CO_2 at 37 °C. MNK-3 cells were obtained from Maria Ciofani (Duke University) and maintained as previously described[35], adding recombinant mouse IL-7 (10 ng/ml; BioLegend) and IL-15 (10 ng/ml; BioLegend) every 3 days. After confirming no mycoplasma contamination, MNK-3 cells were authenticated by their ability to elicit the appropriate cytokine responses following stimulation as originally described[35]. Cells (5×10^5) were plated in 24-well plates. The following day, cells were treated with bacterial supernatants (10% v/v) or EPS (0.5

mg/ml) for 4 hours and lysed for RNA isolation. For experiments with MNK-3 cells, bacterial supernatants were prepared by growing bacteria anaerobically in PYG overnight at 37 °C, resuspending the bacteria in an equal volume of peptone water (10 g/L peptone, 5 g/L sodium chloride), incubating anaerobically overnight at 37 °C, and collecting the supernatants after centrifugation.

Ex vivo cytokine analysis

C57BL/6 mice were orally treated with either sterile PYG or ~10^8 CFU of *C. immunis*. One week later, 4 mm ileal biopsies were collected and incubated in 1 ml of Advanced DMEM F12 + 5% heat inactivated FBS + antibiotics (10 μg/ml colistin, 10 μg/ml doxycycline, 250 μg/ml amphotericin B). The samples that came from the control animals were treated with 50 μl of PYG, and the samples that came from the *C. immunis*-treated animals were treated with ~10^7 CFU of *C. immunis*. After 24 hours incubation in a humidified incubator with 5% CO_2 at 37 °C, the supernatants were collected. The overall viability of the biopsy samples was assessed with a resazurin assay. ELISAs for IL-22 and GM-CSF (BioLegend) were performed according to the manufacturer's instructions.

IL-22 depletion

Mice were injected intraperitoneally with either a neutralizing antibody against IL-22 (150 μg/dose; clone 8E11; Genentech) or an IgG1 isotype control (150 μg/dose; Genentech) every other day. The antibody dosing regimen began 2 days prior to treatment with *C. immunis*.

Phylogeny of *C. immunis licABC* homologs

Homologs of the *C. immunis licABC* locus were identified using BLASTn (2.13.0). The gene sequences for these *licABC* loci as well as the sequences from select organisms primarily found in the respiratory tract were aligned using ClustalW. A maximum likelihood phylogenetic tree was generated using RAxML as implemented with the default settings in MegAlign Pro (DNA Star).

Meta-analysis of *licC* abundances in human studies

We obtained publicly available human-derived shotgun metagenomic data from the curatedMetagenomicData R package (version 3.6.2)[89]. We included all studies available as of July 2023 that had stool samples from westernized countries for which there were corresponding BMI and/or serum triglyceride data. We required samples to be labeled as "control" for "study condition" and "healthy" for "disease." To ensure independence in the dataset (i.e., having only one sample per subject), we included only the baseline sample (or the first entry when no timepoint information was provided) for studies with multiple samples per subject. Additionally, for individuals included in multiple studies, we only included their data from one study. For the BMI analysis, we defined groups as heathy (BMI < 25 kg/m^2), overweight (25 kg/m^2 ≤ BMI < 30 kg/m^2), or obese (BMI ≥ 30 kg/m^2), and we required studies to have ≥10 obese or non-obese subjects, which resulted in a total of 11 studies (total of 4,145 individuals) being combined for this meta-analysis[90-100]. For the serum triglyceride analysis, we defined groups as normal (triglyceride < 150 mg/dL), borderline (150 mg/dL ≤ triglyceride < 200 mg/dL), or high (triglyceride ≥ 200 mg/dL), and we required studies to have ≥10 subjects, which resulted in a total of 4 studies (total of 247 individuals) being combined for this meta-analysis[94,101-103].

We downloaded HUMAnN3-processed UniRef90 gene family abundance tables for each of these studies and scaled them to copies per million. To identify homologs of the *licC* gene, we used the *C. immunis licC* gene sequence to search for UniRef90 entries in the UniProt Knowledgebase[104], setting a similarity threshold of ≥40%. We used the grep UNIX command to extract the abundance of these *licC* homologs from the study-associated data, and we summed their abundances.

Statistics

Sample-size estimates for each experiment were based on previous laboratory experience. The investigators were not blinded to allocation during experiments and outcome assessment. Prism 10 (GraphPad Software) was used for all statistical analyses unless otherwise specified, and the specific statistical tests used are included in the figure legends.

Data Availability

The genome sequences for *C. immunis*, *C. symbiosum*, and *C. clostridioforme* have been deposited at GenBank under accession number xxxxx. The RNAseq data have been deposited to NCBI under BioProject accession number xxxxx.

REFERENCES

1. Federation, W.O. World Obesity Atlas 2023. https://data.worldobesity.org/publications/?cat=19.
2. Collaborators, G.B.D.O., Afshin, A., Forouzanfar, M.H., Reitsma, M.B., Sur, P., Estep, K., Lee, A., Marczak, L., Mokdad, A.H., Moradi-Lakeh, M., et al. (2017). Health Effects of Overweight and Obesity in 195 Countries over 25 Years. N. Engl. J. Med. *377*, 13-27. 10.1056/NEJMoa1614362.
3. Mohebi, R., Chen, C., Ibrahim, N.E., McCarthy, C.P., Gaggin, H.K., Singer, D.E., Hyle, E.P., Wasfy, J.H., and Januzzi, J.L., Jr. (2022). Cardiovascular Disease Projections in the United States Based on the 2020 Census Estimates. J. Am. Coll. Cardiol. *80*, 565-578. 10.1016/j.jacc.2022.05.033.
4. Gutin, I. (2018). In BMI We Trust: Reframing the Body Mass Index as a Measure of Health. Soc Theory Health *16*, 256-271. 10.1057/s41285-017-0055-0.
5. Nuttall, F.Q. (2015). Body Mass Index: Obesity, BMI, and Health: A Critical Review. Nutr Today *50*, 117-128. 10.1097/NT.0000000000000092.
6. Romero-Corral, A., Somers, V.K., Sierra-Johnson, J., Thomas, R.J., Collazo-Clavell, M.L., Korinek, J., Allison, T.G., Batsis, J.A., Sert-Kuniyoshi, F.H., and Lopez-Jimenez, F. (2008). Accuracy of body mass index in diagnosing obesity in the adult general population. Int J Obes (Lond) *32*, 959-966. 10.1038/ijo.2008.11.
7. Tomiyama, A.J., Hunger, J.M., Nguyen-Cuu, J., and Wells, C. (2016). Misclassification of cardiometabolic health when using body mass index categories in NHANES 2005-2012. Int J Obes (Lond) *40*, 883-886. 10.1038/ijo.2016.17.
8. Montague, C.T., and O'Rahilly, S. (2000). The perils of portliness: causes and consequences of visceral adiposity. Diabetes *49*, 883-888. 10.2337/diabetes.49.6.883.
9. Neeland, I.J., Turer, A.T., Ayers, C.R., Powell-Wiley, T.M., Vega, G.L., Farzaneh-Far, R., Grundy, S.M., Khera, A., McGuire, D.K., and de Lemos, J.A. (2012). Dysfunctional adiposity and the risk of prediabetes and type 2 diabetes in obese adults. JAMA *308*, 1150-1159. 10.1001/2012.jama.11132.
10. Vague, J. (1956). The degree of masculine differentiation of obesities: a factor determining predisposition to diabetes, atherosclerosis, gout, and uric calculous disease. Am. J. Clin. Nutr. *4*, 20-34. 10.1093/ajcn/4.1.20.
11. Neeland, I.J., Ross, R., Despres, J.P., Matsuzawa, Y., Yamashita, S., Shai, I., Seidell, J., Magni, P., Santos, R.D., Arsenault, B., et al. (2019). Visceral and ectopic fat, atherosclerosis, and cardiometabolic disease: a position statement. Lancet Diabetes Endocrinol *7*, 715-725. 10.1016/S2213-8587(19)30084-1.
12. Backhed, F., Ding, H., Wang, T., Hooper, L.V., Koh, G.Y., Nagy, A., Semenkovich, C.F., and Gordon, J.I. (2004). The gut microbiota as an environmental factor that regulates fat storage. Proc. Natl. Acad. Sci. U. S. A. *101*, 15718-15723. 10.1073/pnas.0407076101.
13. Suarez-Zamorano, N., Fabbiano, S., Chevalier, C., Stojanovic, O., Colin, D.J., Stevanovic, A., Veyrat-Durebex, C., Tarallo, V., Rigo, D., Germain, S., et al. (2015). Microbiota depletion promotes browning of white adipose tissue and reduces obesity. Nat. Med. *21*, 1497-1501. 10.1038/nm.3994.
14. Virtue, A.T., McCright, S.J., Wright, J.M., Jimenez, M.T., Mowel, W.K., Kotzin, J.J., Joannas, L., Basavappa, M.G., Spencer, S.P., Clark, M.L., et al. (2019). The gut microbiota regulates white adipose tissue inflammation and obesity via a family of microRNAs. Sci. Transl. Med. *11*. 10.1126/scitranslmed.aav1892.
15. Turnbaugh, P.J., Ley, R.E., Mahowald, M.A., Magrini, V., Mardis, E.R., and Gordon, J.I. (2006). An obesity-associated gut microbiome with increased capacity for energy harvest. Nature *444*, 1027-1031. 10.1038/nature05414.
16. Godinho-Silva, C., Domingues, R.G., Rendas, M., Raposo, B., Ribeiro, H., da Silva, J.A., Vieira, A., Costa, R.M., Barbosa-Morais, N.L., Carvalho, T., and Veiga-Fernandes, H. (2019). Light-

entrained and brain-tuned circadian circuits regulate ILC3s and gut homeostasis. Nature *574*, 254-258. 10.1038/s41586-019-1579-3.
17. Kawano, Y., Edwards, M., Huang, Y., Bilate, A.M., Araujo, L.P., Tanoue, T., Atarashi, K., Ladinsky, M.S., Reiner, S.L., Wang, H.H., et al. (2022). Microbiota imbalance induced by dietary sugar disrupts immune-mediated protection from metabolic syndrome. Cell *185*, 3501-3519 e3520. 10.1016/j.cell.2022.08.005.
18. Mao, K., Baptista, A.P., Tamoutounour, S., Zhuang, L., Bouladoux, N., Martins, A.J., Huang, Y., Gerner, M.Y., Belkaid, Y., and Germain, R.N. (2018). Innate and adaptive lymphocytes sequentially shape the gut microbiota and lipid metabolism. Nature *554*, 255-259. 10.1038/nature25437.
19. Wang, Y., Kuang, Z., Yu, X., Ruhn, K.A., Kubo, M., and Hooper, L.V. (2017). The intestinal microbiota regulates body composition through NFIL3 and the circadian clock. Science *357*, 912-916. 10.1126/science.aan0677.
20. Surana, N.K., and Kasper, D.L. (2017). Moving beyond microbiome-wide associations to causal microbe identification. Nature *552*, 244-247. 10.1038/nature25019.
21. Coburn, C.T., Knapp, F.F., Jr., Febbraio, M., Beets, A.L., Silverstein, R.L., and Abumrad, N.A. (2000). Defective uptake and utilization of long chain fatty acids in muscle and adipose tissues of CD36 knockout mice. J. Biol. Chem. *275*, 32523-32529. 10.1074/jbc.M003826200.
22. Cohen, P., Miyazaki, M., Socci, N.D., Hagge-Greenberg, A., Liedtke, W., Soukas, A.A., Sharma, R., Hudgins, L.C., Ntambi, J.M., and Friedman, J.M. (2002). Role for stearoyl-CoA desaturase-1 in leptin-mediated weight loss. Science *297*, 240-243. 10.1126/science.1071527.
23. Cai, L., Wang, Z., Ji, A., Meyer, J.M., and van der Westhuyzen, D.R. (2012). Scavenger receptor CD36 expression contributes to adipose tissue inflammation and cell death in diet-induced obesity. PLoS One *7*, e36785. 10.1371/journal.pone.0036785.
24. Sasaki, T., Moro, K., Kubota, T., Kubota, N., Kato, T., Ohno, H., Nakae, S., Saito, H., and Koyasu, S. (2019). Innate Lymphoid Cells in the Induction of Obesity. Cell Rep *28*, 202-217 e207. 10.1016/j.celrep.2019.06.016.
25. Henke, M.T., Kenny, D.J., Cassilly, C.D., Vlamakis, H., Xavier, R.J., and Clardy, J. (2019). Ruminococcus gnavus, a member of the human gut microbiome associated with Crohn's disease, produces an inflammatory polysaccharide. Proc. Natl. Acad. Sci. U. S. A. *116*, 12672-12677. 10.1073/pnas.1904099116.
26. Mazmanian, S.K., Liu, C.H., Tzianabos, A.O., and Kasper, D.L. (2005). An immunomodulatory molecule of symbiotic bacteria directs maturation of the host immune system. Cell *122*, 107-118. 10.1016/j.cell.2005.05.007.
27. Surana, N.K., and Kasper, D.L. (2012). The yin yang of bacterial polysaccharides: lessons learned from B. fragilis PSA. Immunol. Rev. *245*, 13-26. 10.1111/j.1600-065X.2011.01075.x.
28. Garcia-Rubio, R., de Oliveira, H.C., Rivera, J., and Trevijano-Contador, N. (2020). The Fungal Cell Wall: Candida, Cryptococcus, and Aspergillus Species. Frontiers in Microbiology *10*. 10.3389/fmicb.2019.02993.
29. Voiniciuc, C., Dama, M., Gawenda, N., Stritt, F., and Pauly, M. (2019). Mechanistic insights from plant heteromannan synthesis in yeast. Proceedings of the National Academy of Sciences *116*, 522-527. doi:10.1073/pnas.1814003116.
30. Clark, S.E., and Weiser, J.N. (2013). Microbial modulation of host immunity with the small molecule phosphorylcholine. Infect. Immun. *81*, 392-401. 10.1128/IAI.01168-12.
31. Waller, M.C., Bober, J.R., Nair, N.U., and Beisel, C.L. (2017). Toward a genetic tool development pipeline for host-associated bacteria. Curr. Opin. Microbiol. *38*, 156-164. 10.1016/j.mib.2017.05.006.
32. Guo, C.-J., Allen, B.M., Hiam, K.J., Dodd, D., Van Treuren, W., Higginbottom, S., Nagashima, K., Fischer, C.R., Sonnenburg, J.L., Spitzer, M.H., and Fischbach, M.A. (2019). Depletion of microbiome-derived molecules in the host using Clostridium genetics. Science *366*, eaav1282. doi:10.1126/science.aav1282.

33. McAllister, K.N., Bouillaut, L., Kahn, J.N., Self, W.T., and Sorg, J.A. (2017). Using CRISPR-Cas9-mediated genome editing to generate C. difficile mutants defective in selenoproteins synthesis. Scientific Reports *7*, 14672. 10.1038/s41598-017-15236-5.
34. Zhao, J., Fang, H., and Zhang, D. (2020). Expanding application of CRISPR-Cas9 system in microorganisms. Synthetic and Systems Biotechnology *5*, 269-276. https://doi.org/10.1016/j.synbio.2020.08.001.
35. Allan, D.S., Kirkham, C.L., Aguilar, O.A., Qu, L.C., Chen, P., Fine, J.H., Serra, P., Awong, G., Gommerman, J.L., Zuniga-Pflucker, J.C., and Carlyle, J.R. (2015). An in vitro model of innate lymphoid cell function and differentiation. Mucosal Immunol. *8*, 340-351. 10.1038/mi.2014.71.
36. Song, C., Lee, J.S., Gilfillan, S., Robinette, M.L., Newberry, R.D., Stappenbeck, T.S., Mack, M., Cella, M., and Colonna, M. (2015). Unique and redundant functions of NKp46+ ILC3s in models of intestinal inflammation. Journal of Experimental Medicine *212*, 1869-1882. 10.1084/jem.20151403.
37. Kawano, Y., Edwards, M., Huang, Y., Bilate, A.M., Araujo, L.P., Tanoue, T., Atarashi, K., Ladinsky, M.S., Reiner, S.L., Wang, H.H., et al. (2022). Microbiota imbalance induced by dietary sugar disrupts immune-mediated protection from metabolic syndrome. Cell. https://doi.org/10.1016/j.cell.2022.08.005.
38. Eberl, G., and Littman, D.R. (2004). Thymic origin of intestinal alphabeta T cells revealed by fate mapping of RORgammat+ cells. Science *305*, 248-251. 10.1126/science.1096472.
39. Qiu, J., Guo, X., Chen, Z.M., He, L., Sonnenberg, G.F., Artis, D., Fu, Y.X., and Zhou, L. (2013). Group 3 innate lymphoid cells inhibit T-cell-mediated intestinal inflammation through aryl hydrocarbon receptor signaling and regulation of microflora. Immunity *39*, 386-399. 10.1016/j.immuni.2013.08.002.
40. Song, C., Lee, J.S., Gilfillan, S., Robinette, M.L., Newberry, R.D., Stappenbeck, T.S., Mack, M., Cella, M., and Colonna, M. (2015). Unique and redundant functions of NKp46+ ILC3s in models of intestinal inflammation. J. Exp. Med. *212*, 1869-1882. 10.1084/jem.20151403.
41. Mortha, A., Chudnovskiy, A., Hashimoto, D., Bogunovic, M., Spencer, S.P., Belkaid, Y., and Merad, M. (2014). Microbiota-dependent crosstalk between macrophages and ILC3 promotes intestinal homeostasis. Science *343*, 1249288. 10.1126/science.1249288.
42. Sanos, S.L., Bui, V.L., Mortha, A., Oberle, K., Heners, C., Johner, C., and Diefenbach, A. (2009). RORgammat and commensal microflora are required for the differentiation of mucosal interleukin 22-producing NKp46+ cells. Nat. Immunol. *10*, 83-91. 10.1038/ni.1684.
43. Pearson, C., Thornton, E.E., McKenzie, B., Schaupp, A.L., Huskens, N., Griseri, T., West, N., Tung, S., Seddon, B.P., Uhlig, H.H., and Powrie, F. (2016). ILC3 GM-CSF production and mobilisation orchestrate acute intestinal inflammation. eLife *5*, e10066. 10.7554/eLife.10066.
44. Gaudino, S.J., Beaupre, M., Lin, X., Joshi, P., Rathi, S., McLaughlin, P.A., Kempen, C., Mehta, N., Eskiocak, O., Yueh, B., et al. (2021). IL-22 receptor signaling in Paneth cells is critical for their maturation, microbiota colonization, Th17-related immune responses, and anti-Salmonella immunity. Mucosal Immunol. *14*, 389-401. 10.1038/s41385-020-00348-5.
45. Young, N.M., Foote, S.J., and Wakarchuk, W.W. (2013). Review of phosphocholine substituents on bacterial pathogen glycans: synthesis, structures and interactions with host proteins. Mol. Immunol. *56*, 563-573. 10.1016/j.molimm.2013.05.237.
46. Pasolli, E., Schiffer, L., Manghi, P., Renson, A., Obenchain, V., Truong, D.T., Beghini, F., Malik, F., Ramos, M., Dowd, J.B., et al. (2017). Accessible, curated metagenomic data through ExperimentHub. Nat Methods *14*, 1023-1024. 10.1038/nmeth.4468.
47. Choi, W.J., Dong, H.J., Jeong, H.U., Ryu, D.W., Song, S.M., Kim, Y.R., Jung, H.H., Kim, T.H., and Kim, Y.H. (2020). Lactobacillus plantarum LMT1-48 exerts anti-obesity effect in high-fat diet-induced obese mice by regulating expression of lipogenic genes. Sci Rep *10*, 869. 10.1038/s41598-020-57615-5.
48. Everard, A., Belzer, C., Geurts, L., Ouwerkerk, J.P., Druart, C., Bindels, L.B., Guiot, Y., Derrien, M., Muccioli, G.G., Delzenne, N.M., et al. (2013). Cross-talk between Akkermansia muciniphila

and intestinal epithelium controls diet-induced obesity. Proc. Natl. Acad. Sci. U. S. A. *110*, 9066-9071. 10.1073/pnas.1219451110.
49. Goodrich, J.K., Waters, J.L., Poole, A.C., Sutter, J.L., Koren, O., Blekhman, R., Beaumont, M., Van Treuren, W., Knight, R., Bell, J.T., et al. (2014). Human genetics shape the gut microbiome. Cell *159*, 789-799. 10.1016/j.cell.2014.09.053.
50. Miyoshi, M., Ogawa, A., Higurashi, S., and Kadooka, Y. (2014). Anti-obesity effect of Lactobacillus gasseri SBT2055 accompanied by inhibition of pro-inflammatory gene expression in the visceral adipose tissue in diet-induced obese mice. Eur. J. Nutr. *53*, 599-606. 10.1007/s00394-013-0568-9.
51. Whitfield, C., Wear, S.S., and Sande, C. (2020). Assembly of Bacterial Capsular Polysaccharides and Exopolysaccharides. Annu. Rev. Microbiol. *74*, 521-543. 10.1146/annurev-micro-011420-075607.
52. Sender, R., Fuchs, S., and Milo, R. (2016). Are We Really Vastly Outnumbered? Revisiting the Ratio of Bacterial to Host Cells in Humans. Cell *164*, 337-340. 10.1016/j.cell.2016.01.013.
53. Bertozzi, C.R., and Rabuka, D. (2009). Structural basis of glycan diversity. In Essentials of Glycobiology, A. Varki, R.D. Cummings, J.D. Esko, H.H. Freeze, P. Stanley, C.R. Bertozzi, G.W. Hart, and M.E. Etzler, eds. (Cold Spring Harbor Laboratory Press).
54. Dube, D.H., Champasa, K., and Wang, B. (2011). Chemical tools to discover and target bacterial glycoproteins. Chem Commun (Camb) *47*, 87-101. 10.1039/c0cc01557a.
55. Porter, N.T., and Martens, E.C. (2017). The Critical Roles of Polysaccharides in Gut Microbial Ecology and Physiology. Annu. Rev. Microbiol. *71*, 349-369. 10.1146/annurev-micro-102215-095316.
56. Volanakis, J.E., and Kaplan, M.H. (1971). Specificity of C-reactive protein for choline phosphate residues of pneumococcal C-polysaccharide. Proc. Soc. Exp. Biol. Med. *136*, 612-614. 10.3181/00379727-136-35323.
57. Weiser, J.N., Shchepetov, M., and Chong, S.T. (1997). Decoration of lipopolysaccharide with phosphorylcholine: a phase-variable characteristic of Haemophilus influenzae. Infect. Immun. *65*, 943-950. 10.1128/IAI.65.3.943-950.1997.
58. Cundell, D.R., Gerard, N.P., Gerard, C., Idanpaan-Heikkila, I., and Tuomanen, E.I. (1995). Streptococcus pneumoniae anchor to activated human cells by the receptor for platelet-activating factor. Nature *377*, 435-438. 10.1038/377435a0.
59. Serino, L., and Virji, M. (2002). Genetic and functional analysis of the phosphorylcholine moiety of commensal Neisseria lipopolysaccharide. Mol. Microbiol. *43*, 437-448. 10.1046/j.1365-2958.2002.02755.x.
60. Swords, W.E., Buscher, B.A., Ver Steeg Ii, K., Preston, A., Nichols, W.A., Weiser, J.N., Gibson, B.W., and Apicella, M.A. (2000). Non-typeable Haemophilus influenzae adhere to and invade human bronchial epithelial cells via an interaction of lipooligosaccharide with the PAF receptor. Mol. Microbiol. *37*, 13-27. 10.1046/j.1365-2958.2000.01952.x.
61. Pang, B., Winn, D., Johnson, R., Hong, W., West-Barnette, S., Kock, N., and Swords, W.E. (2008). Lipooligosaccharides containing phosphorylcholine delay pulmonary clearance of nontypeable Haemophilus influenzae. Infect. Immun. *76*, 2037-2043. 10.1128/IAI.01716-07.
62. Weiser, J.N., Pan, N., McGowan, K.L., Musher, D., Martin, A., and Richards, J. (1998). Phosphorylcholine on the lipopolysaccharide of Haemophilus influenzae contributes to persistence in the respiratory tract and sensitivity to serum killing mediated by C-reactive protein. J. Exp. Med. *187*, 631-640. 10.1084/jem.187.4.631.
63. Kharat, A.S., and Tomasz, A. (2006). Drastic reduction in the virulence of Streptococcus pneumoniae expressing type 2 capsular polysaccharide but lacking choline residues in the cell wall. Mol. Microbiol. *60*, 93-107. 10.1111/j.1365-2958.2006.05082.x.
64. Clark, S.E., Snow, J., Li, J., Zola, T.A., and Weiser, J.N. (2012). Phosphorylcholine allows for evasion of bactericidal antibody by Haemophilus influenzae. PLoS Pathog *8*, e1002521. 10.1371/journal.ppat.1002521.

65. Lysenko, E., Richards, J.C., Cox, A.D., Stewart, A., Martin, A., Kapoor, M., and Weiser, J.N. (2000). The position of phosphorylcholine on the lipopolysaccharide of Haemophilus influenzae affects binding and sensitivity to C-reactive protein-mediated killing. Mol. Microbiol. *35*, 234-245. 10.1046/j.1365-2958.2000.01707.x.
66. Tzianabos, A.O., Onderdonk, A.B., Rosner, B., Cisneros, R.L., and Kasper, D.L. (1993). Structural features of polysaccharides that induce intra-abdominal abscesses. Science *262*, 416-419.
67. Neff, C.P., Rhodes, M.E., Arnolds, K.L., Collins, C.B., Donnelly, J., Nusbacher, N., Jedlicka, P., Schneider, J.M., McCarter, M.D., Shaffer, M., et al. (2016). Diverse Intestinal Bacteria Contain Putative Zwitterionic Capsular Polysaccharides with Anti-inflammatory Properties. Cell Host Microbe *20*, 535-547. 10.1016/j.chom.2016.09.002.
68. Tzianabos, A.O., Wang, J.Y., and Lee, J.C. (2001). Structural rationale for the modulation of abscess formation by Staphylococcus aureus capsular polysaccharides. Proc. Natl. Acad. Sci. U. S. A. *98*, 9365-9370. 10.1073/pnas.161175598.
69. Young, N.M., Kreisman, L.S., Stupak, J., Maclean, L.L., Cobb, B.A., and Richards, J.C. (2011). Structural characterization and MHCII-dependent immunological properties of the zwitterionic O-chain antigen of Morganella morganii. Glycobiology. 10.1093/glycob/cwr018.
70. Cobb, B.A., Wang, Q., Tzianabos, A.O., and Kasper, D.L. (2004). Polysaccharide processing and presentation by the MHCII pathway. Cell *117*, 677-687. 10.016/j.cell.2004.05.001.
71. Zou, J., Chassaing, B., Singh, V., Pellizzon, M., Ricci, M., Fythe, M.D., Kumar, M.V., and Gewirtz, A.T. (2018). Fiber-Mediated Nourishment of Gut Microbiota Protects against Diet-Induced Obesity by Restoring IL-22-Mediated Colonic Health. Cell Host Microbe *23*, 41-53 e44. 10.1016/j.chom.2017.11.003.
72. Upadhyay, V., Poroyko, V., Kim, T.J., Devkota, S., Fu, S., Liu, D., Tumanov, A.V., Koroleva, E.P., Deng, L., Nagler, C., et al. (2012). Lymphotoxin regulates commensal responses to enable diet-induced obesity. Nat. Immunol. *13*, 947-953. 10.1038/ni.2403.
73. Park, O., Ki, S.H., Xu, M., Wang, H., Feng, D., Tam, J., Osei-Hyiaman, D., Kunos, G., and Gao, B. (2015). Biologically active, high levels of interleukin-22 inhibit hepatic gluconeogenesis but do not affect obesity and its metabolic consequences. Cell Biosci *5*, 25. 10.1186/s13578-015-0015-0.
74. Wang, X., Ota, N., Manzanillo, P., Kates, L., Zavala-Solorio, J., Eidenschenk, C., Zhang, J., Lesch, J., Lee, W.P., Ross, J., et al. (2014). Interleukin-22 alleviates metabolic disorders and restores mucosal immunity in diabetes. Nature *514*, 237-241. 10.1038/nature13564.
75. Walisser, J.A., Glover, E., Pande, K., Liss, A.L., and Bradfield, C.A. (2005). Aryl hydrocarbon receptor-dependent liver development and hepatotoxicity are mediated by different cell types. Proc. Natl. Acad. Sci. U. S. A. *102*, 17858-17863. 10.1073/pnas.0504757102.
76. Mombaerts, P., Iacomini, J., Johnson, R.S., Herrup, K., Tonegawa, S., and Papaioannou, V.E. (1992). RAG-1-deficient mice have no mature B and T lymphocytes. Cell *68*, 869-877. 10.1016/0092-8674(92)90030-g.
77. Robb, L., Drinkwater, C.C., Metcalf, D., Li, R., Kontgen, F., Nicola, N.A., and Begley, C.G. (1995). Hematopoietic and lung abnormalities in mice with a null mutation of the common beta subunit of the receptors for granulocyte-macrophage colony-stimulating factor and interleukins 3 and 5. Proc. Natl. Acad. Sci. U. S. A. *92*, 9565-9569. 10.1073/pnas.92.21.9565.
78. Chung, H., Pamp, Sünje J., Hill, Jonathan A., Surana, Neeraj K., Edelman, Sanna M., Troy, Erin B., Reading, Nicola C., Villablanca, Eduardo J., Wang, S., Mora, Jorge R., et al. (2012). Gut Immune Maturation Depends on Colonization with a Host-Specific Microbiota. Cell *149*, 1578-1593. https://doi.org/10.1016/j.cell.2012.04.037.
79. Dobin, A., Davis, C.A., Schlesinger, F., Drenkow, J., Zaleski, C., Jha, S., Batut, P., Chaisson, M., and Gingeras, T.R. (2012). STAR: ultrafast universal RNA-seq aligner. Bioinformatics *29*, 15-21. 10.1093/bioinformatics/bts635.

80. Liao, Y., Smyth, G.K., and Shi, W. (2013). featureCounts: an efficient general purpose program for assigning sequence reads to genomic features. Bioinformatics *30*, 923-930. 10.1093/bioinformatics/btt656.
81. Love, M.I., Huber, W., and Anders, S. (2014). Moderated estimation of fold change and dispersion for RNA-seq data with DESeq2. Genome Biology *15*, 550. 10.1186/s13059-014-0550-8.
82. Subramanian, A., Tamayo, P., Mootha, V.K., Mukherjee, S., Ebert, B.L., Gillette, M.A., Paulovich, A., Pomeroy, S.L., Golub, T.R., Lander, E.S., and Mesirov, J.P. (2005). Gene set enrichment analysis: A knowledge-based approach for interpreting genome-wide expression profiles. Proceedings of the National Academy of Sciences *102*, 15545-15550. doi:10.1073/pnas.0506580102.
83. Mina, A.I., LeClair, R.A., LeClair, K.B., Cohen, D.E., Lantier, L., and Banks, A.S. (2018). CalR: A Web-Based Analysis Tool for Indirect Calorimetry Experiments. Cell Metab *28*, 656-666 e651. 10.1016/j.cmet.2018.06.019.
84. Kolmogorov, M., Yuan, J., Lin, Y., and Pevzner, P.A. (2019). Assembly of long, error-prone reads using repeat graphs. Nature Biotechnology *37*, 540-546. 10.1038/s41587-019-0072-8.
85. Aziz, R.K., Bartels, D., Best, A.A., DeJongh, M., Disz, T., Edwards, R.A., Formsma, K., Gerdes, S., Glass, E.M., Kubal, M., et al. (2008). The RAST Server: Rapid Annotations using Subsystems Technology. BMC Genomics *9*, 75. 10.1186/1471-2164-9-75.
86. Santander, J., Martin, T., Loh, A., Pohlenz, C., Gatlin, D.M., and Curtiss, R. (2013). Mechanisms of intrinsic resistance to antimicrobial peptides of Edwardsiella ictaluri and its influence on fish gut inflammation and virulence. Microbiology (Reading) *159*, 1471-1486. 10.1099/mic.0.066639-0.
87. Heiss, C., Klutts, J.S., Wang, Z., Doering, T.L., and Azadi, P. (2009). The structure of Cryptococcus neoformans galactoxylomannan contains beta-D-glucuronic acid. Carbohydr. Res. *344*, 915-920. 10.1016/j.carres.2009.03.003.
88. Heap, J.T., Pennington, O.J., Cartman, S.T., and Minton, N.P. (2009). A modular system for Clostridium shuttle plasmids. Journal of Microbiological Methods *78*, 79-85. https://doi.org/10.1016/j.mimet.2009.05.004.
89. Pasolli, E., Schiffer, L., Manghi, P., Renson, A., Obenchain, V., Truong, D.T., Beghini, F., Malik, F., Ramos, M., Dowd, J.B., et al. (2017). Accessible, curated metagenomic data through ExperimentHub. Nature Methods *14*, 1023-1024. 10.1038/nmeth.4468.
90. Asnicar, F., Berry, S.E., Valdes, A.M., Nguyen, L.H., Piccinno, G., Drew, D.A., Leeming, E., Gibson, R., Le Roy, C., Khatib, H.A., et al. (2021). Microbiome connections with host metabolism and habitual diet from 1,098 deeply phenotyped individuals. Nat. Med. *27*, 321-332. 10.1038/s41591-020-01183-8.
91. Costea, P.I., Coelho, L.P., Sunagawa, S., Munch, R., Huerta-Cepas, J., Forslund, K., Hildebrand, F., Kushugulova, A., Zeller, G., and Bork, P. (2017). Subspecies in the global human gut microbiome. Mol Syst Biol *13*, 960. 10.15252/msb.20177589.
92. Hansen, L.B.S., Roager, H.M., Sondertoft, N.B., Gobel, R.J., Kristensen, M., Valles-Colomer, M., Vieira-Silva, S., Ibrugger, S., Lind, M.V., Maerkedahl, R.B., et al. (2018). A low-gluten diet induces changes in the intestinal microbiome of healthy Danish adults. Nat Commun *9*, 4630. 10.1038/s41467-018-07019-x.
93. Human Microbiome Project, C. (2012). Structure, function and diversity of the healthy human microbiome. Nature *486*, 207-214. 10.1038/nature11234.
94. Jie, Z., Xia, H., Zhong, S.L., Feng, Q., Li, S., Liang, S., Zhong, H., Liu, Z., Gao, Y., Zhao, H., et al. (2017). The gut microbiome in atherosclerotic cardiovascular disease. Nat Commun *8*, 845. 10.1038/s41467-017-00900-1.
95. Keohane, D.M., Ghosh, T.S., Jeffery, I.B., Molloy, M.G., O'Toole, P.W., and Shanahan, F. (2020). Microbiome and health implications for ethnic minorities after enforced lifestyle changes. Nat. Med. *26*, 1089-1095. 10.1038/s41591-020-0963-8.

96. Le Chatelier, E., Nielsen, T., Qin, J., Prifti, E., Hildebrand, F., Falony, G., Almeida, M., Arumugam, M., Batto, J.M., Kennedy, S., et al. (2013). Richness of human gut microbiome correlates with metabolic markers. Nature *500*, 541-546. 10.1038/nature12506.
97. Nielsen, H.B., Almeida, M., Juncker, A.S., Rasmussen, S., Li, J., Sunagawa, S., Plichta, D.R., Gautier, L., Pedersen, A.G., Le Chatelier, E., et al. (2014). Identification and assembly of genomes and genetic elements in complex metagenomic samples without using reference genomes. Nat. Biotechnol. *32*, 822-828. 10.1038/nbt.2939.
98. Xie, H., Guo, R., Zhong, H., Feng, Q., Lan, Z., Qin, B., Ward, K.J., Jackson, M.A., Xia, Y., Chen, X., et al. (2016). Shotgun Metagenomics of 250 Adult Twins Reveals Genetic and Environmental Impacts on the Gut Microbiome. Cell Syst *3*, 572-584 e573. 10.1016/j.cels.2016.10.004.
99. Zeevi, D., Korem, T., Zmora, N., Israeli, D., Rothschild, D., Weinberger, A., Ben-Yacov, O., Lador, D., Avnit-Sagi, T., Lotan-Pompan, M., et al. (2015). Personalized Nutrition by Prediction of Glycemic Responses. Cell *163*, 1079-1094. 10.1016/j.cell.2015.11.001.
100. Zhernakova, A., Kurilshikov, A., Bonder, M.J., Tigchelaar, E.F., Schirmer, M., Vatanen, T., Mujagic, Z., Vila, A.V., Falony, G., Vieira-Silva, S., et al. (2016). Population-based metagenomics analysis reveals markers for gut microbiome composition and diversity. Science *352*, 565-569. 10.1126/science.aad3369.
101. Feng, Q., Liang, S., Jia, H., Stadlmayr, A., Tang, L., Lan, Z., Zhang, D., Xia, H., Xu, X., Jie, Z., et al. (2015). Gut microbiome development along the colorectal adenoma-carcinoma sequence. Nat Commun *6*, 6528. 10.1038/ncomms7528.
102. Karlsson, F.H., Tremaroli, V., Nookaew, I., Bergstrom, G., Behre, C.J., Fagerberg, B., Nielsen, J., and Backhed, F. (2013). Gut metagenome in European women with normal, impaired and diabetic glucose control. Nature *498*, 99-103. 10.1038/nature12198.
103. Yu, J., Feng, Q., Wong, S.H., Zhang, D., Liang, Q.Y., Qin, Y., Tang, L., Zhao, H., Stenvang, J., Li, Y., et al. (2017). Metagenomic analysis of faecal microbiome as a tool towards targeted non-invasive biomarkers for colorectal cancer. Gut *66*, 70-78. 10.1136/gutjnl-2015-309800.
104. The UniProt, C. (2023). UniProt: the Universal Protein Knowledgebase in 2023. Nucleic Acids Research *51*, D523-D531. 10.1093/nar/gkac1052.

Figure 1

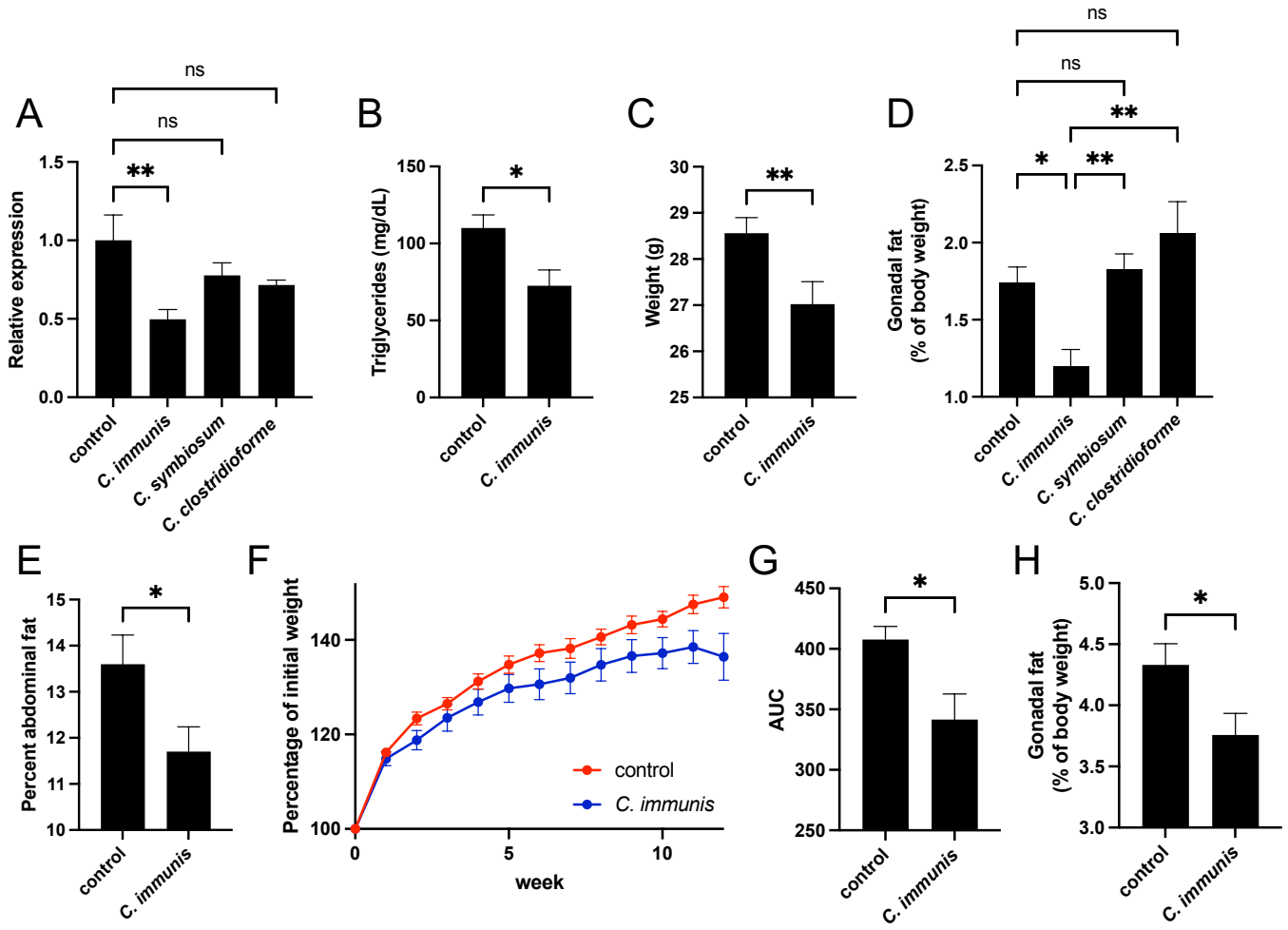
A
ns
ns
**
Relative expression
1.5
1.0
0.5
0.0
control
C. immunis
C. symbiosum
C. clostridioforme
B
*
Triglycerides (mg/dL)
150
100
50
0
control
C. immunis
C
**
Weight (g)
30
29
28
27
26
25
control
C. immunis
D
ns
ns
**
*
**
Gonadal fat
(% of body weight)
2.5
2.0
1.5
1.0
control
C. immunis
C. symbiosum
C. clostridioforme
E
*
Percent abdominal fat
15
14
13
12
11
10
control
C. immunis
F
Percentage of initial weight
140
120
100
0
5
10
week
control
C. immunis
G
*
AUC
450
400
350
300
250
control
C. immunis
H
*
Gonadal fat
(% of body weight)
5.0
4.5
4.0
3.5
3.0
control
C. immunis

Figure 2

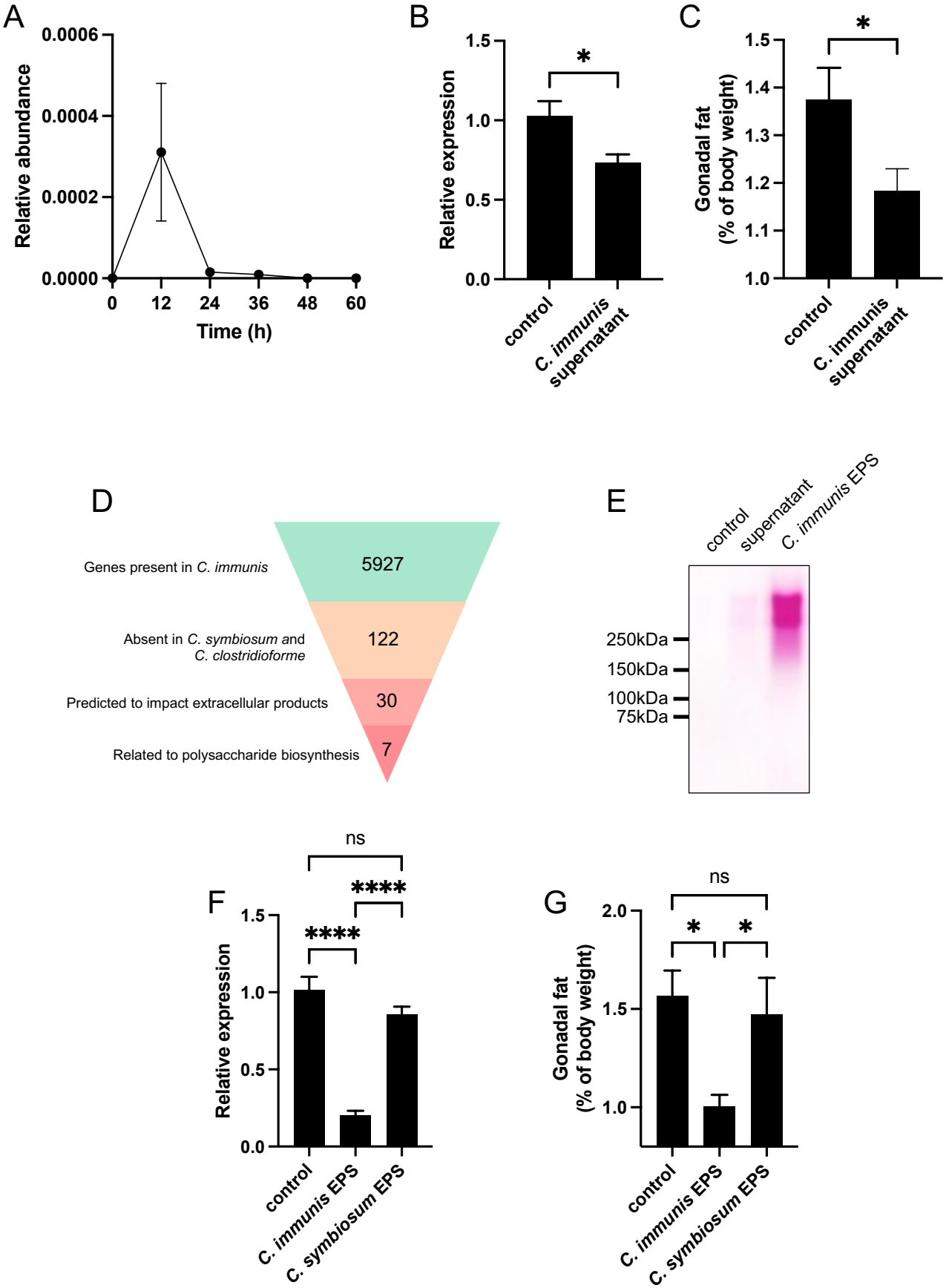
A
Relative abundance
0.0006
0.0004
0.0002
0.0000
0
12
24
36
48
60
Time (h)
B
Relative expression
1.5
1.0
0.5
0.0
*
control
C. immunis supernatant
C
Gonadal fat (% of body weight)
1.5
1.4
1.3
1.2
1.1
1.0
*
control
C. immunis supernatant
D
Genes present in C. immunis
5927
Absent in C. symbiosum and C. clostridioforme
122
Predicted to impact extracellular products
30
Related to polysaccharide biosynthesis
7
E
control
supernatant
C. immunis EPS
250kDa
150kDa
100kDa
75kDa
F
Relative expression
1.5
1.0
0.5
0.0
ns
****
****
control
C. immunis EPS
C. symbiosum EPS
G
Gonadal fat (% of body weight)
2.0
1.5
1.0
ns
*
*
control
C. immunis EPS
C. symbiosum EPS

Figure 3

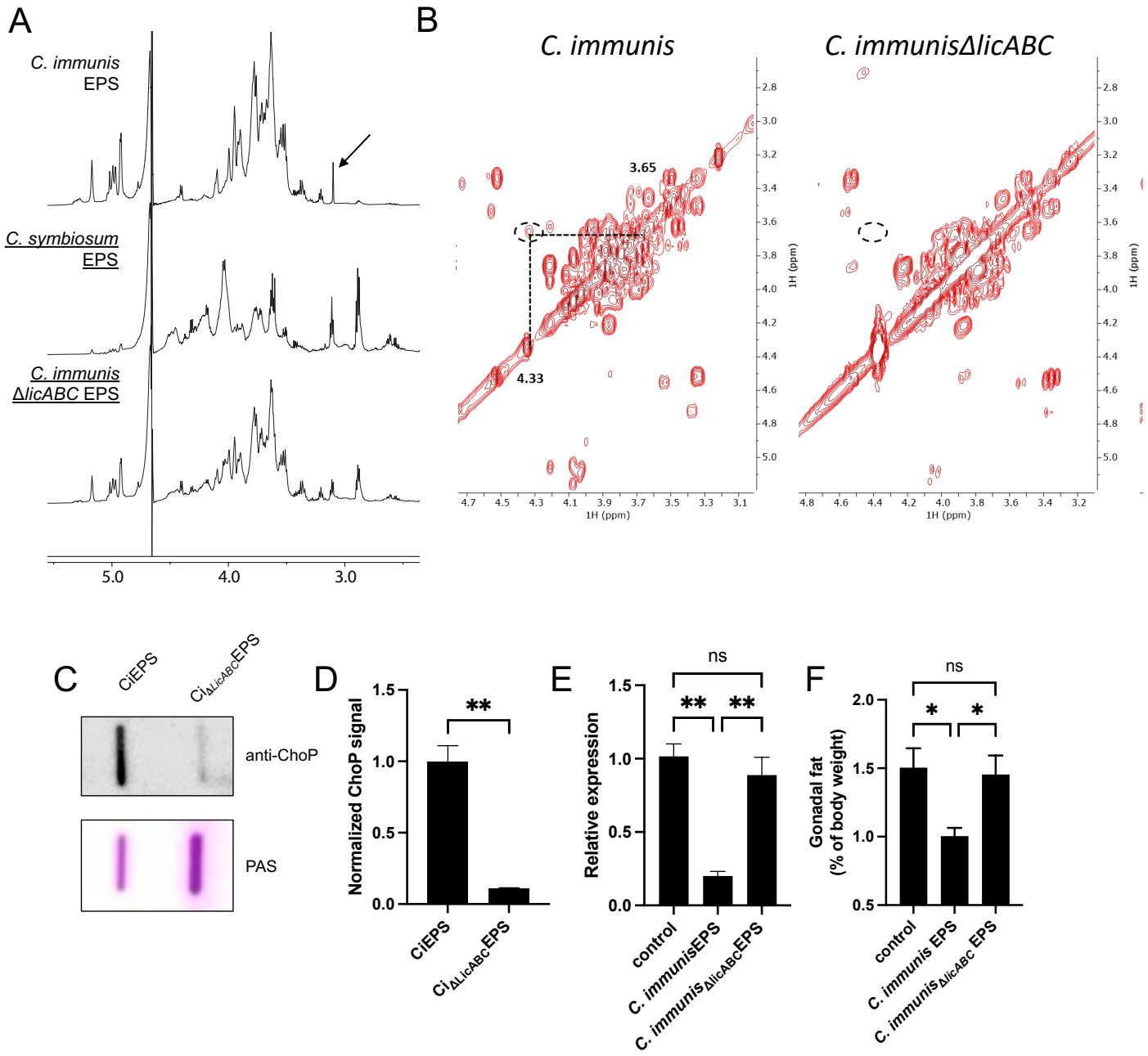
A
C. immunis EPS
C. symbiosum EPS
C. immunis ΔlicABC EPS
5.0
4.0
3.0
B
C. immunis
C. immunisΔlicABC
3.65
4.33
1H (ppm)
C
CiEPS
CiΔLicABCEPS
anti-ChoP
PAS
D
Normalized ChoP signal
**
CiEPS
CiΔLicABCEPS
E
Relative expression
ns
**
**
control
C. immunisEPS
C. immunisΔlicABCEPS
F
Gonadal fat (% of body weight)
ns
*
*
control
C. immunis EPS
C. immunisΔlicABC EPS

Figure 4

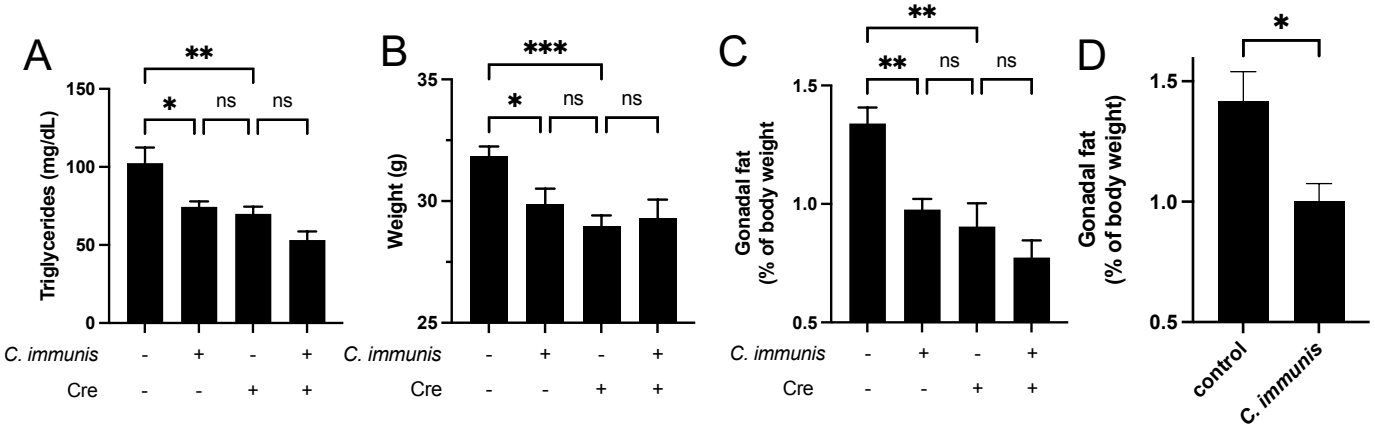
A
Triglycerides (mg/dL)
150
100
50
0
**
*
ns
ns
C. immunis - + - +
Cre - - + +
B
Weight (g)
35
30
25
***
*
ns
ns
C. immunis - + - +
Cre - - + +
C
Gonadal fat
(% of body weight
1.5
1.0
0.5
**
**
ns
ns
C. immunis - + - +
Cre - - + +
D
Gonadal fat
(% of body weight)
1.5
1.0
0.5
*
control
C. immunis

Figure 5

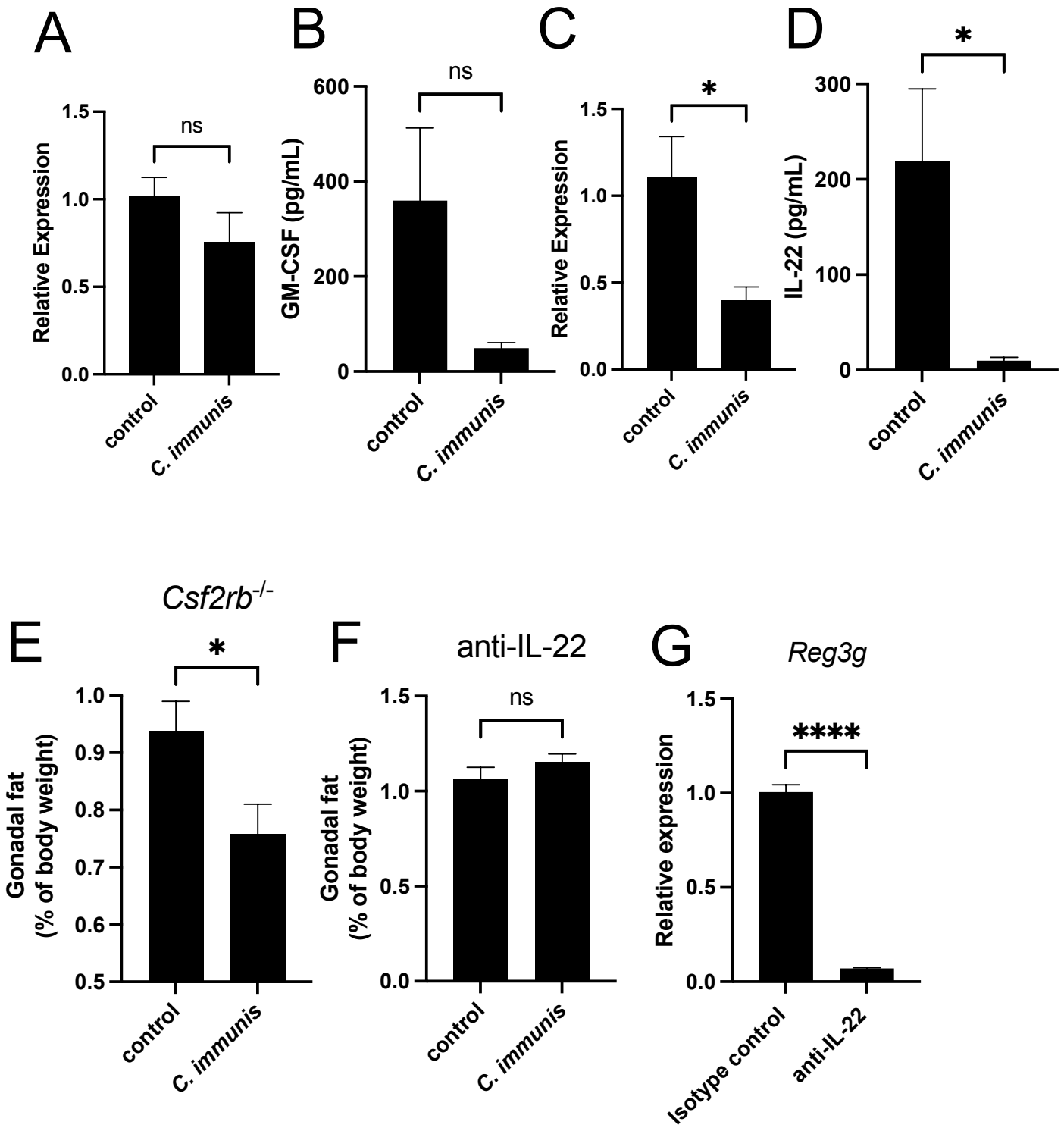
A
Relative Expression
1.5
1.0
0.5
0.0
ns
control
C. immunis
B
GM-CSF (pg/mL)
600
400
200
0
ns
control
C. immunis
C
Relative Expression
1.5
1.0
0.5
0.0
*
control
C. immunis
D
IL-22 (pg/mL)
300
200
100
0
*
control
C. immunis
Csf2rb-/-
E
Gonadal fat
(% of body weight)
1.0
0.9
0.8
0.7
0.6
0.5
*
control
C. immunis
F
anti-IL-22
Gonadal fat
(% of body weight)
1.5
1.0
0.5
0.0
ns
control
C. immunis
G
Reg3g
Relative expression
1.5
1.0
0.5
0.0
****
Isotype control
anti-IL-22

Figure 6

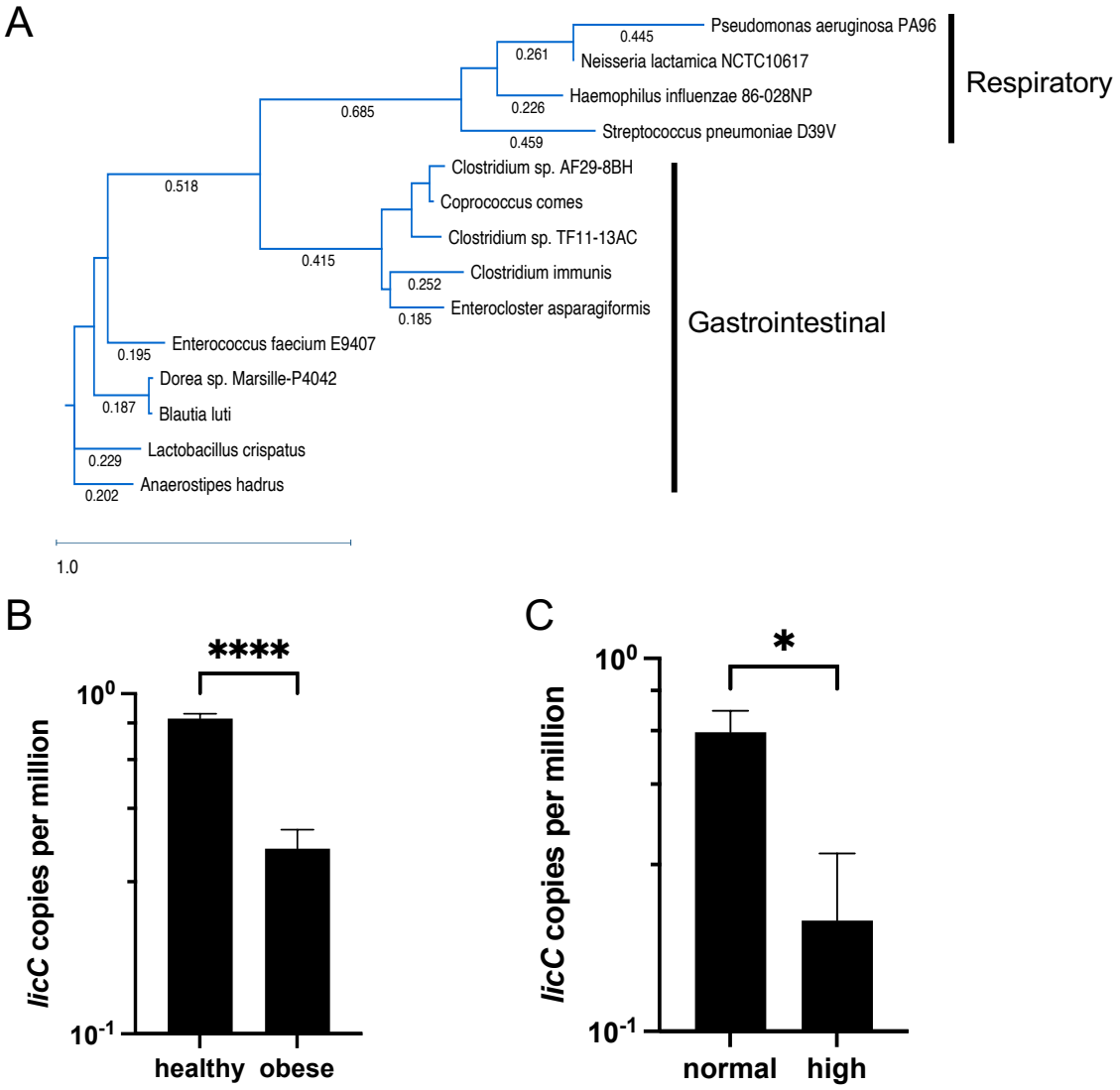
A
Pseudomonas aeruginosa PA96
Neisseria lactamica NCTC10617
Haemophilus influenzae 86-028NP
Streptococcus pneumoniae D39V
Respiratory
Clostridium sp. AF29-8BH
Coprococcus comes
Clostridium sp. TF11-13AC
Clostridium immunis
Enterocloster asparagiformis
Enterococcus faecium E9407
Dorea sp. Marsille-P4042
Blautia luti
Lactobacillus crispatus
Anaerostipes hadrus
Gastrointestinal
0.445
0.261
0.226
0.459
0.685
0.518
0.415
0.252
0.185
0.195
0.187
0.229
0.202
1.0
B
****
licC copies per million
healthy
obese
C
*
licC copies per million
normal
high